

On the long-term correlation between the flux in the Ca II H & K and H α lines for FGK stars

J. Gomes da Silva^{1,2}, N.C. Santos^{1,2}, I. Boisse¹, X. Dumusque^{1,3}, and C. Lovis³

¹ Centro de Astrofísica, Universidade do Porto, Rua das Estrelas, 4150-762 Porto, Portugal
e-mail: Joao.Silva@astro.up.pt

² Departamento de Física e Astronomia, Faculdade de Ciências, Universidade do Porto, Portugal

³ Observatoire de Genève, Université de Genève, 51 ch. des Maillettes, CH-1290 Versoix, Switzerland

Received date / Accepted date

ABSTRACT

The re-emission in the cores of the Ca II H & K and H α lines, are well known proxies of stellar activity. However, these activity indices probe different activity phenomena, the first being more sensitive to plage variation, while the other one being more sensitive to filaments. In this paper we study the long-term correlation between $\log R'_{HK}$ and $\log I_{H\alpha}$, two indices based on the Ca II H & K and H α lines respectively, for a sample of 271 FGK stars using measurements obtained over a ~ 9 year time span. Because stellar activity is one of the main obstacles to the detection of low-mass and long-period planets, understanding further this activity index correlation can give us some hints about the optimal target to focus on, and ways to correct for these activity effects.

We found a great variety of long-term correlations between $\log R'_{HK}$ and $\log I_{H\alpha}$. Around 20% of our sample has strong positive correlation between the indices while about 3% show strong negative correlation. These fractions are compatible with those found for the case of early-M dwarfs. Stars exhibiting a positive correlation have a tendency to be more active when compared to the median of the sample, while stars showing a negative correlation are more present among higher metallicity stars.

There is also a tendency for the positively correlated stars to be more present among the coolest stars, a result which is probably due to the activity level effect on the correlation. Activity level and metallicity seem therefore to be playing a role on the correlation between $\log R'_{HK}$ and $\log I_{H\alpha}$. Possible explanations based on the influence of filaments for the diversity in the correlations between these indices are discussed in this paper. As a parallel result, we show a way to estimate the effective temperature of FGK dwarfs exhibiting a low activity level by using the H α index.

Key words. Keywords should be given

1. Introduction

Stellar activity is one of the main limitations to the detection of low-mass and/or long-period planets using the radial-velocity method (e.g. Saar & Donahue 1997; Santos et al. 2000; Queloz et al. 2001; Boisse et al. 2009, 2011; Dumusque et al. 2011b; Lovis et al. 2011; Gomes da Silva et al. 2012). Fortunately, the radial-velocity noise induced by these effects can, in some cases, be corrected for example if the activity is simultaneously measured using activity indices (e.g. Dumusque et al. 2011a, 2012). Therefore, understanding the behaviour of activity indices and their relation with radial-velocity is vital to reduce the impact of activity in radial-velocity measurements and thus improve its sensitivity to planetary signals.

The re-emission in the Ca II H & K lines are widely used proxies of activity induced signals in radial-velocity measurements. However, for solar-type stars, the relation between this index and H α is not well understood. Since these two activity indices are affected by different activity phenomena in different ways (the emission in the centre of the Ca II and H α lines are not formed at the same temperature in the chromosphere), understanding their relationship and differences might bring new insights not only to stellar physics but also to the detection and characterisation of extrasolar planets.

It is known that there is a long-term correlation between the emission in the Ca II H & K and H α lines that follow the Sun's 11-year activity cycle (Livingston et al. 2007). Other au-

thors have suggested that the correlation is also present in other stars (Giampapa et al. 1989; Robinson et al. 1990; Strassmeier et al. 1990; Pasquini & Pallavicini 1991; Montes et al. 1995). However, when Cincunegui et al. (2007) measured simultaneously the flux in the two lines for a sample of 109 southern FGK and M stars, they found a large scatter in correlations, from very strong positive correlations to negative ones. They also suggested that the mean values of the flux in the Ca II and H α lines are correlated due to the effect of stellar colour on both fluxes.

Meunier & Delfosse (2009) studied the contribution of plagues and filaments to the emission in Ca II and H α lines during a solar cycle. In their work, plagues contributes to an increase in emission in both fluxes while filaments increases absorption in H α only. They found that the contribution of filaments to H α can be responsible for the decrease in the correlation coefficient between the two fluxes depending on their spatial distribution and contrast compared to those of plagues. They also noted that at higher activity levels (e.g. cycle maxima), the filament filling factor saturates and the correlation between the two fluxes increases. Other factors contributing to a decrease in the measured correlation can be the time-span of observations, cycle phase at which they are measured, and stellar inclination angle. For example, if the time-span is less than the cycle period (or the activity range is not well spanned) the correlation will probably be underestimated.

Santos et al. (2010) studied the long-term activity of 8 FGK stars using the Ca II H & K based S_{MW} and H α indices and found

a general long-term correlation between the two. However their sample was not large enough to have any statistical significance. Gomes da Silva et al. (2011) expanded the comparison between these two activity sensitive lines to early-M dwarfs. Similarly to Cincunegui et al. (2007) they detected a large variety of correlation coefficients, including anti-correlations for the least active stars in their sample. The most active stars were all, however, positively correlated. They also found hints that in some cases the H α index was following an "anti-cycle" relative to their *S*-index, i.e., the maxima and minima measured in the two indices were anti-correlated. However, their time-span was not long enough to detect full cycles and confirm this effect.

In this paper, we analyse the behaviour of the flux in Ca II H & K and H α lines in FGK stars via two activity indices corrected for the effects of photospheric flux. We describe our sample and data in Sect. 2. The activity indices derivation, statistics, correlations between mean values, and activity cycle detectability are presented in Sect. 3 and Appendix A. The correlations between the two indices are discussed in Sect. 4. The distribution of the correlations in mean values of activity are discussed in Sect. 5. The effects of metallicity on the correlation are studied in Sect. 6, and the distribution of the correlations in effective temperature is presented in Sect. 7. We discuss possible causes for the existence of positive correlations and anti-correlations, and compare our results with those found for early-M dwarfs in Sect. 8, and finally conclude in Sect. 9. A possible use of the H α index to estimate the effective temperature of low activity level FGK dwarfs is proposed in Appendix B.

2. Sample and data

The sample comes from the ~ 400 FGK stars HARPS (spectral resolution = 115 000) high-precision sample already used by Lovis et al. (2011) to study the long-term activity of FGK stars and its effect on the measurement of precise radial velocities. A description of the sample is presented in their paper. The spectra used in this work were obtained between February 2003 and February 2012. We used effective temperature, metallicity, and surface gravity that were already calculated for this sample by Sousa et al. (2008). Absolute magnitude and luminosity were both obtained from the Hipparcos catalogue.

We selected only spectra with $S/N \geq 100$ at spectral order 56 (~ 5870 Å), and nightly averaged our measurements. Only stars with 10 or more nights of observations were selected. Then, we selected just the Main Sequence (MS) stars as in Lovis et al. (2011): we fitted a straight line through the H-R diagram and then excluded all stars with luminosity greater than +0.25 dex above that line.

We ended up with 271 MS stars with a median time span of ~ 7 years that we used for the rest of this work. This sample is comprised of 11,432 data points, with a median of 23 nights of observations per star (and a maximum of 279). The sample ranges in spectral type from F8 to K6, in effective temperature from 4595 to 6276 K, and in metallicity from -0.84 to $+0.39$ dex.

3. The activity indices

The $\log R'_{HK}$ index, which is already corrected for the photospheric flux (Noyes et al. 1984), and respective errors were directly obtained from the HARPS DRS. This index is based on the *S*-index which is calculated as the sum of the flux in two 0.6 Å bands centered at the calcium H (3968.47 Å) and K (3933.66

Å) lines divided by two 20 Å reference bands centered at 3900 and 4000 Å (see e.g. Boisse et al. 2009).

The H α index and errors were calculated as in Gomes da Silva et al. (2011). We used a 1.6 Å band centered at 6562.808 Å and divided the flux in the central line by the flux in two reference bands of 10.75 and 8.75 Å centered at 6550.87 and 6580.31 Å, respectively. The flux errors were calculated as the photon noise in the line core, \sqrt{N} , where N is the number of photons in the band. The activity indices errors were obtained via error propagation. The calibration of H α for the effects of photospheric flux is presented in Appendix A and results in the $I_{H\alpha}$ index.

3.1. Statistics of the $\log R'_{HK}$ index

Our sample, which is biased towards inactive stars in order to increase the chances of finding low-mass planets, has a median $\log R'_{HK}$ of -4.948 and a mean of -4.923 . In this 271-star sample, only 22 (around 8%) are considered active stars, with $\log R'_{HK} \geq -4.75$, lying on the higher activity region above the "Vaughan-Preston gap" (Vaughan & Preston 1980).

The star with the highest activity level is HD224789, with $\log R'_{HK} = -4.433$ and the most inactive star is HD181433 with $\log R'_{HK} = -5.144$. The median of the errors obtained for the $\log R'_{HK}$ index is 0.003, or in relative terms, 0.06% around the mean. In terms of variability, the median standard deviation of the sample is 0.0154 (0.3% around the mean), with HD177758 being the least variable star with $\sigma(\log R'_{HK}) = 0.0035$ (0.07% around the mean) and HD7199 the star that varies the most with $\sigma(\log R'_{HK}) = 0.08$ (1.6% around the mean).

3.2. Statistics of the $\log I_{H\alpha}$ index

In terms of $\log I_{H\alpha}$, our sample has a median value of -1.7129 and a mean of -1.7118 . The star with the highest $\log I_{H\alpha}$ mean value is HD85119, with an activity level of -1.6562 and the most inactive star is HD82516 with $\log I_{H\alpha} = -1.7299$. The median of the errors we obtained for the $\log I_{H\alpha}$ index is 0.0002, or in relative terms, 0.01% around the mean. As stated before, we are only considering photon noise as a source of errors, and since the H α line is in a brighter area of the spectrum compared to the Ca II H & K lines, we expect the photon noise to be lower for $I_{H\alpha}$ than for R'_{HK} . In terms of variability, the median standard deviation of the sample is 0.0019 (0.11% around the mean), with HD74014 being the least variable star with $\sigma(\log I_{H\alpha}) = 0.0008$ (0.05% around the mean) and HD224789 the star that varies the most with $\sigma(\log I_{H\alpha}) = 0.0063$ (0.4% around the mean).

From these simple statistics we can see that the $\log R'_{HK}$ is more sensitive to activity variations than $\log I_{H\alpha}$. While $\log R'_{HK}$ has a median standard deviation of 0.3% of the mean, $\log I_{H\alpha}$ only has a median standard deviation of 0.1% of the mean, which means that $\log R'_{HK}$ will have a more noticeable variation.

3.3. Mean activity level correlations

Our activity indices are corrected for the effects of photospheric flux, and can, if they are not dependent on other factors other than chromospheric flux, be used to compare the activity levels between different stars. Figure 1 (upper panel) shows the correlation between the mean values of $\log R'_{HK}$ and $\log I_{H\alpha}$. These mean values were calculated by averaging the two indices over all our nightly measurements, and represent the average activity level of each star. Open triangles are stars with correlation coef-

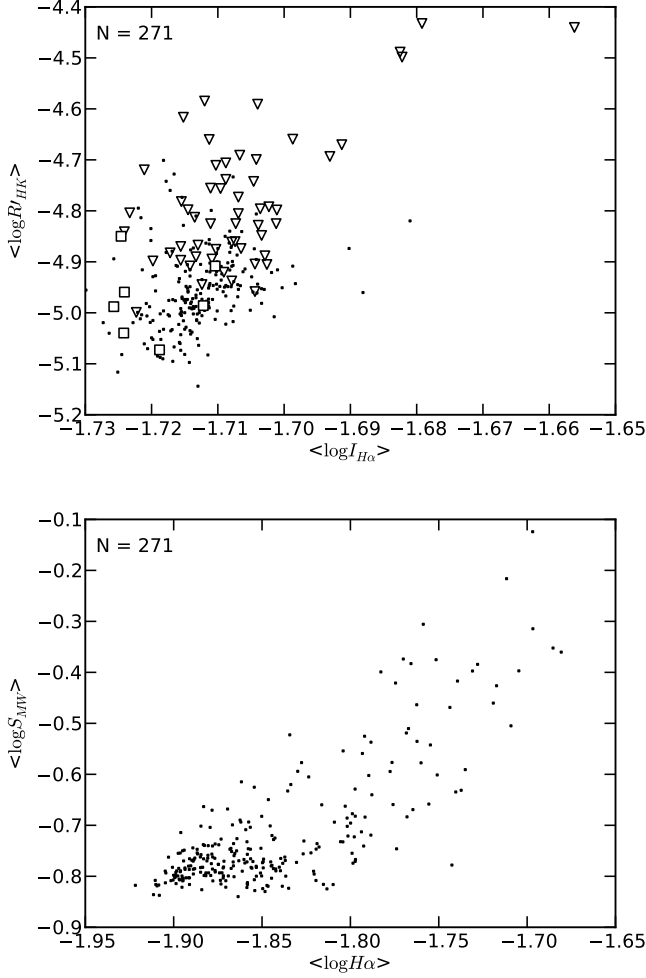


Fig. 1: *Upper panel*: Relationship between $\log R'_{HK}$ and $\log I_{H\alpha}$ mean activity levels. Open triangles are stars with positive correlation between the two indices with $\rho \geq 0.5$, open squares stars with negative correlation with $\rho \leq -0.5$, and dots stars with no correlations. *Lower panel*: Relationship between the logarithms of S_{MW} and H α indices.

efficient, $\rho \geq 0.5$, squares are stars with $\rho \leq -0.5$, and dots stars with no strong correlations. There is a correlation between the indices, with a correlation coefficient of 0.53, but the scatter is large and the relation appears not to be linear (c.f. Cincunegui et al. 2007, Fig. 12). However, if we choose only the positively correlated stars (open triangles), they show a slightly more well defined relationship for the mean values with a correlation coefficient of 0.65. When Cincunegui et al. (2007) studied the correlation between the mean values of the flux in Ca II and H α they concluded that the correlation between them is due to the dependence of the mean fluxes on stellar colour. Indeed, when we plot the logarithm of the mean indices S_{MW} vs. H α (without colour correction), we have a stronger correlation with $\rho = 0.79$ (Fig. 1, lower panel). We can therefore confirm that stellar colour is playing a role in the correlation between the mean flux levels of the Ca II and H α lines.

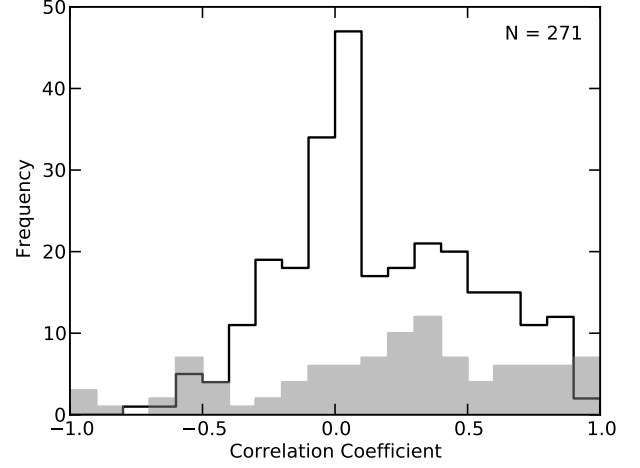


Fig. 2: Distribution of correlation coefficients between $\log R'_{HK}$ and $\log I_{H\alpha}$ for the whole sample (black line). The grey filled histogram shows the distribution of correlations for the 101 stars in Cincunegui et al. (2007) sample that have their correlations calculated.

3.4. Activity cycles: detectability

To detect activity cycles we fitted sinusoids to the time-series of the two activity indices. The significance of the fitting process was addressed by using an F-test where $F = \sigma_{const}^2 / \sigma_{sin}^2$ to compare the fitting of a sinusoid with that of a constant model with σ being the standard deviation of the residuals of the fitted model. The probability $p(F)$ will give the probability that the data is better fitted by a constant model than a sinusoidal function. We selected stars with cycles as the ones where probabilities, $p(F)_{HK}$ and $p(F)_{H\alpha}$, are lower than 0.05 and, similarly to Lovis et al. (2011), we searched for periods in the region between 2 and 11 years.

Based on this selection criteria and using $\log R'_{HK}$, we detected 69 stars (26%) with significant activity cycles with periods varying between 2.0 and 10.8 years. The $\log I_{H\alpha}$ index, however, is not so sensitive at detecting magnetic cycles. Only 9 stars (3.3%) showed significant cycles with periods varying between 3.9 and 9.5 years. As a comparison, Robertson et al. (2013) detected activity cycles with periods longer than one year in 5% of their sample of 93 K5-M5 stars using an H α index similar to ours. In their study of activity cycles based on this sample but with a different selection criteria, Lovis et al. (2011) found that, out of their 284-star sample, 99 stars (35%) showed long-term activity cycles in their $\log R'_{HK}$ index. Their slightly higher fraction of stars with cycles is probably due to the fact that they use a different selection criteria with a different restriction on the number of data points (some of their stars with detected cycles have less than 10 observations), we use only data with $S/N \geq 100$, and we have more data points.

4. Correlations between $\log R'_{HK}$ and $\log I_{H\alpha}$

For all stars we calculated the Pearson correlation coefficient between $\log R'_{HK}$ and $\log I_{H\alpha}$. As was detected by Cincunegui et al. (2007) for the flux in the Ca II H & K and H α lines, we also find a great variety of correlation coefficients between $\log R'_{HK}$ and $\log I_{H\alpha}$, in the range $-0.78 \leq \rho \leq 0.95$ (Fig. 2). Although there is a tendency for the stronger correlations to be positive, we found a few cases of anti-correlations with $\rho \leq -0.5$.

Since we are interested in studying the cases of strong long-term correlations between the flux in the Ca II H & K and H α lines, we made a new selection of stars with good quality data that we are going to describe in the following section.

4.1. Stars with "strong" long-term correlations

We are interested in measuring the long-term Pearson correlation coefficient (ρ) between the $\log R'_{HK}$ and $\log I_{H\alpha}$ indices. We need therefore to ensure that we have (a) a long time-span to certify that we are measuring long-term variations², (b) variability in the long-term so that we are not measuring correlations due to noise, (c) no short-term variations that can interfere with or hide the long-term ones, (d) enough quantity of points to calculate a significant ρ , and (e) strong correlations. To achieve this, we perform the following selection criteria on our 271-star sample:

1. All data was binned into 100-day averages, each bin with at least three nights of observations, where the errors were calculated as the standard error on the mean, σ/\sqrt{N} , where σ is the standard deviation of the observations and N the number of observations. This will reduce the variation induced by short-term activity modulated by stellar rotation.
2. We selected stars with at least four bins. This selection ensures that we have enough points to calculate ρ and that the time span is at least 400 days.
3. Only stars that showed long-term variability in $\log R'_{HK}$ were selected. This will ensure that we are not detecting random variations due to noise. We performed an F -test on the binned data where $F = \sigma_e^2/\langle\sigma_i\rangle^2$, with σ_e the standard deviation of the binned data and $\langle\sigma_i\rangle$ the mean of the errors on the bins (e.g. Zechmeister et al. 2009). We calculated the probability of the F -test, $P(F)$, that the variations are due to the internal errors of the binned data, and selected stars with $P(F) \leq 0.05$ (95% probability that the variability is not due to the internal errors).
4. We also applied the variability F -test for the $\log I_{H\alpha}$ index in a similar way as described above.
5. To select significant correlation coefficients between $\log R'_{HK}$ and $\log I_{H\alpha}$ we calculated the False Alarm Probability (FAP) of having absolute values of ρ higher than the ones obtained for each star by bootstrapping the binned data and calculating the fraction of cases with higher $|\rho|$ values. We used 10000 permutations per star to calculate the FAP values. Only stars with $FAP \leq 0.05$ (95% significance level) were selected.

¹ We should note that for 165 stars they do not find cycles but they cannot exclude cycles either. In their conclusions they arrive at a final value of 61% of stars with cycles when they exclude these stars from the fraction.

² Since this sample derives from a planet hunt selection of stars, active stars with $\log R'_{HK} \geq -4.7$ were monitored early and only rarely measured. Therefore, stars with higher activity will have fewer measurements and possibly a lower time-span of observations. This selection will thus reduce even more the number of active stars in the sample.

6. Stars with strong correlations were selected as the ones having $|\rho| \geq 0.70$.

From the 129 stars that passed selections (1) and (2), 95 stars (73.6%) show long-term variability in $\log R'_{HK}$, 51 stars (39.5%) show long-term variability in $\log I_{H\alpha}$, and 45 stars (34.9%) show long-term variability on both indices. Out of the 45 stars that show variability on both indices, 12 stars (26.7%) show strong positive correlations between the indices, 10 of them (22.2%) having positive correlations while two (4.4%) having anti-correlations.

Table 1 shows the variability and correlations data for the 12 stars with strong long-term correlations, where N_{bins} the number of bins for each star, ρ the correlation coefficient value, FAP the false alarm probability of ρ , and the parameters of the F -tests for both activity indices. The time series of $\log R'_{HK}$, $\log I_{H\alpha}$, and their respective correlations for these 12 stars are shown in Fig. B.2. We also tried to fit sinusoids to these stars (see Sect. 3.4) using the binned data of both indices to check if these stars have significant activity cycles. These fits appear in Fig. B.2 if the $p(F)_{HK}$ of the fit is lower than 0.05 (95% significance level). Two stars, HD100508 and HD78612, only have four bins and therefore do not have enough free parameters to calculate the probability of the fit. From the stars with more than four bins, three have $p(F)$ values lower than 0.05 for the $\log R'_{HK}$ index, namely HD4915, HD63765, and HD88742. These are all stars with strong positive correlations. The 7 stars with significant cycles in $\log R'_{HK}$ have periods in the range 1528 to 10665 days, and 5 of them could be fitted in $\log I_{H\alpha}$ with the same period found for $\log R'_{HK}$ and a $p(F)_{H\alpha}$ value lower than 0.05 (HD13808, HD154577, HD215152, HD7199, and HD85512). For this sample, no star showed a period in $\log I_{H\alpha}$ that was not found also in $\log R'_{HK}$, and at a higher significance.

To try to understand why some stars have positive correlations while others have negative, we compared the correlations with the basic stellar parameters shown in Table 2. The two stars with negative correlations are shown in bold. First, we observe that the two stars with the negative correlations are two of the most inactive in terms of both $\log R'_{HK}$ and $\log I_{H\alpha}$. Second, while all the stars with positive correlation coefficient have negative metallicity (median value of -0.20 dex), the two stars with negative correlations have positive metallicity (median value of 0.34 dex).

Although we can see hints that activity level and metallicity could be influencing the correlation between the two indices, the small number of stars we are using is insufficient to clearly show a solid trend between these parameters. We therefore chose to relax our selection criteria to increase the number of stars in our sample and check if the trends with activity level and metallicity are maintained.

4.2. "Relaxed" selection of stars with correlations

To increase the number of stars in our study we discarded the variability tests, FAPs on the correlation coefficients and used the full data sets based on the nightly averaged data. The correlation coefficient limit was also decreased to $|\rho| \geq 0.5$. This produced a larger sample which will include weaker correlations that can be due to a lower number of data points, shorter time-spans, and/or due to short-term variations. We shall therefore take this part of the study as an indication and not as a proof. However we will now be able to do statistical tests to this sample.

Using this selection, we found that out of the 271 stars in our original sample, 58 (21.4% of the sample) have positive

Table 1: Variability and correlations using binned data for the stars with strong long-term correlations.

Star	N_{bins}	T_{span} [days]	ρ	FAP	$\log R'_{HK}$			$\log I_{H\alpha}$		
					σ_e	$\langle\sigma_i\rangle$	$P(F)$	σ_e	$\langle\sigma_i\rangle$	$P(F)$
HD100508	4	766	-0.93	0.047	0.0199	0.0034	0.0082	0.00102	0.00031	0.040
HD13808	13	2245	0.97	0.0001	0.0794	0.0043	$< 10^{-5}$	0.00302	0.00065	$< 10^{-5}$
HD154577	7	2117	0.92	0.0014	0.0302	0.0030	0.00001	0.00242	0.00047	0.00046
HD209100	7	829	0.92	0.0021	0.0278	0.0048	0.00022	0.00282	0.00088	0.0062
HD215152	9	1160	0.83	0.0034	0.0322	0.0028	$< 10^{-5}$	0.00144	0.00045	0.0016
HD4915	5	646	0.98	0.0046	0.0343	0.0041	0.00062	0.00185	0.00062	0.029
HD63765	8	1936	0.88	0.0024	0.0374	0.0077	0.00023	0.00290	0.00068	0.00052
HD71835	10	2618	0.85	0.0010	0.0403	0.0048	$< 10^{-5}$	0.00165	0.00046	0.00040
HD7199	11	2237	-0.82	0.0009	0.0758	0.0071	$< 10^{-5}$	0.00207	0.00048	0.00003
HD78612	4	2902	0.88	0.050	0.0135	0.0036	0.029	0.00187	0.00057	0.042
HD85512	12	2906	0.93	$< 10^{-4}$	0.0495	0.0026	$< 10^{-5}$	0.00395	0.00052	$< 10^{-5}$
HD88742	5	1729	0.93	0.015	0.0323	0.0043	0.00089	0.00308	0.00086	0.015

Table 2: Stellar parameters of the stars with strong long-term correlations.

Star	$\langle\log R'_{HK}\rangle$	$\langle\log I_{H\alpha}\rangle$	[Fe/H]	T_{eff} [K]	$\log g$ [cm s $^{-2}$]	M_V	$B - V$	P_{rot} [days]
HD100508	-5.055	-1.7198	0.39 ± 0.05	5449 ± 61	4.42 ± 0.09	5.16	0.83	48.4
HD13808	-4.892	-1.7138	-0.20 ± 0.03	5087 ± 41	4.40 ± 0.08	6.08	0.87	42.8
HD154577	-4.878	-1.7019	-0.70 ± 0.02	4900 ± 37	4.52 ± 0.08	6.70	0.89	41.3
HD209100	-4.781	-1.7153	-0.20 ± 0.04	4754 ± 89	4.45 ± 0.19	6.89	1.06	37.2
HD215152	-4.871	-1.7157	-0.10 ± 0.04	4935 ± 76	4.40 ± 0.14	6.45	0.97	42.0
HD4915	-4.798	-1.7038	-0.21 ± 0.01	5658 ± 13	4.52 ± 0.03	5.26	0.66	20.4
HD63765	-4.741	-1.7044	-0.16 ± 0.01	5432 ± 19	4.42 ± 0.03	5.53	0.74	25.0
HD71835	-4.889	-1.7194	-0.04 ± 0.02	5438 ± 22	4.39 ± 0.04	5.38	0.77	35.2
HD7199	-4.946	-1.7270	0.28 ± 0.03	5386 ± 45	4.34 ± 0.08	5.29	0.85	45.9
HD78612	-5.004	-1.7154	-0.24 ± 0.01	5834 ± 14	4.27 ± 0.02	4.06	0.61	21.7
HD85512	-4.898	-1.7023	-0.32 ± 0.03	4715 ± 102	4.39 ± 0.28	7.43	1.16	47.3
HD88742	-4.688	-1.7031	-0.02 ± 0.01	5981 ± 13	4.52 ± 0.02	4.60	0.59	11.4

Notes. The average values of $\log R'_{HK}$ and $\log I_{H\alpha}$ were calculated using the binned data.

correlations between $\log R'_{HK}$ and $\log I_{H\alpha}$, and 8 (3.0% of the sample) have anti-correlations. Table B.1 shows the 66 stars with $|\rho| \geq 0.5$ with their activity mean levels and standard deviations, stellar parameters, and correlation coefficient between the two indices. Stars with correlation coefficients in the range $-0.5 < \rho < 0.5$ (no correlations) are presented in Table B.2.

All the eight stars with negative correlations ($\rho \leq -0.5$) have low $\log R'_{HK}$ activity levels with a median value of -4.97 and a median super-solar metallicity with a value of 0.20. The 58 stars with positive correlations ($\rho \geq 0.5$) have $\log R'_{HK}$ with a median value of -4.81 and a median sub-solar metallicity with a value of -0.16 . This "relaxed" selection appears to maintain the trends found in Section 4.1. In the next sections we will study these trends for this sample of stars.

5. Mean activity level and correlations

Here we investigate the distribution of the positively and negatively correlated stars in terms of $\log R'_{HK}$ and $\log I_{H\alpha}$ activity levels.

Figure 3 (upper panel) shows the distribution of activity as measured by the $\log R'_{HK}$ index. The black line is the histogram of the selected sample of 271 main sequence stars. We can observe the selection bias against active stars as the great majority of the sample lies between -5.1 and -4.8 dex, with a median of -4.95 dex. The hatched and filled grey histograms show the distribution in average activity level of the stars with positive and negative $\log R'_{HK}$ - $\log I_{H\alpha}$ correlations, respectively. The

median of the negatively correlated stars is close to the median of the full sample (but with a tendency to be less active) with a value of -4.97 dex, while the median of the positively correlated stars lies in a higher activity zone, with a value of -4.81 dex. In general, the majority of the least active stars show no strong correlations between the two indices. However, it is obvious from the plot that there is a tendency for the positively correlated stars to be more active in general, and all stars more active than $\log R'_{HK} = -4.7$ have positive correlations between $\log R'_{HK}$ and $\log I_{H\alpha}$. The relative histogram in Fig. 3 (lower panel) illustrates very well this tendency.

The separation between positively and negatively correlated stars is further confirmed by the Kolmogorov-Smirnov (K-S) test that shows that the two populations are distinct with a p -value of 0.002 and a D value³ of 0.664. A similar distribution was found for $\log I_{H\alpha}$ (Fig. 4). The correlation between the two indices have different distributions according to activity level, with negatively correlated stars being the least active ones and the positively correlated stars increasing in number with $I_{H\alpha}$ activity level. In this case, the K-S test have a $D = 0.513$ and p -value = 0.03. The histograms also show that the values in $\log I_{H\alpha}$ are very well constrained between -1.73 and -1.70 , and only a few cases of higher activity stars exists beyond these values. Note that, in the

³ The K-S D value is the highest value of the difference between the cumulative distributions of the two populations. The p -value gives the probability that the two populations come from the same parent distribution.

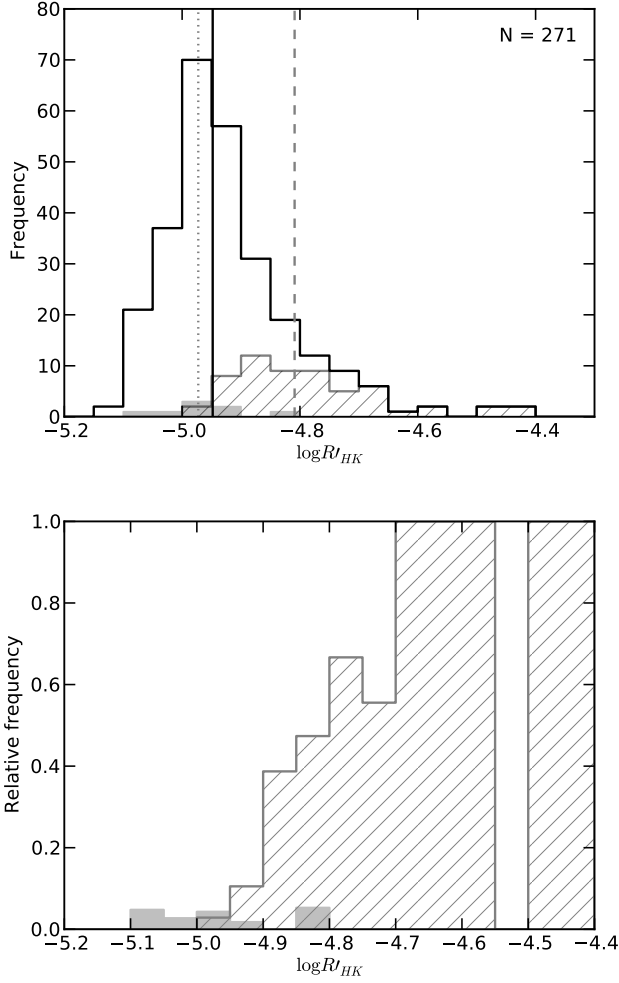


Fig. 3: *Upper panel:* Distribution on $\log R'_{HK}$ activity for the full sample (black), stars with positive correlation coefficient higher than 0.5 (hatched grey), and stars with negative correlation coefficient lower than -0.5 (filled grey). Vertical lines are the medians of the distributions with black line for the full sample, dashed line for positively correlated stars, and dotted line for negatively correlated stars. *Lower panel:* Same as the upper panel but using relative distribution on $\log R'_{HK}$, i.e., the values in each bin are divided by the total number of stars in the respective bin.

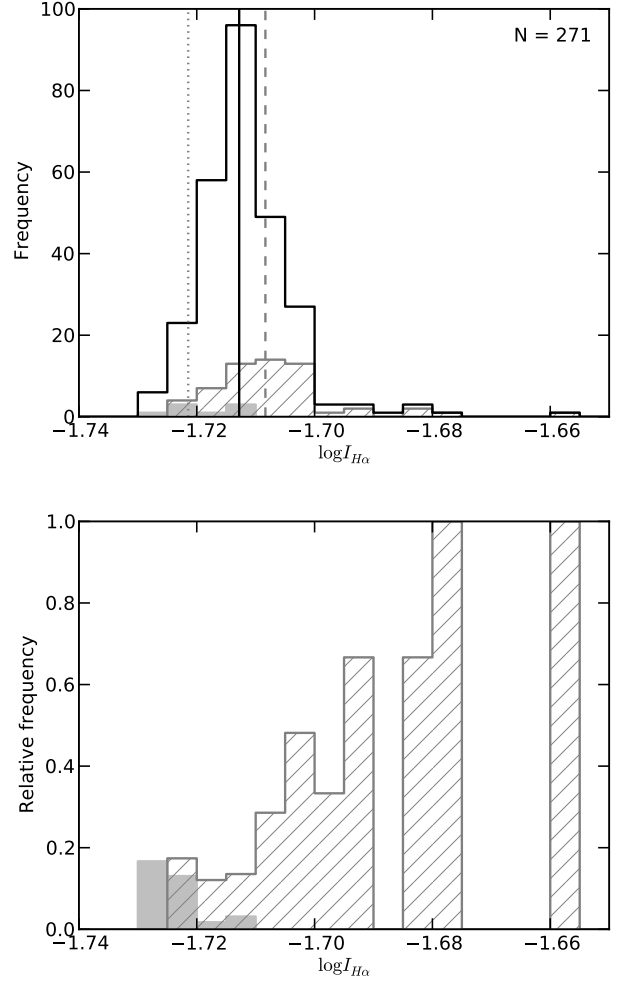


Fig. 4: *Upper panel:* Distribution on $\log I_{H\alpha}$ activity for the full sample (black), stars with positive correlation coefficient higher than 0.5 (hatched grey), and stars with negative correlation coefficient lower than -0.5 (filled grey). Vertical lines are the medians of the distributions with black line for the full sample, dashed line for positively correlated stars, and dotted line for negatively correlated stars. *Lower panel:* Same as the upper panel but using relative distribution on $\log I_{H\alpha}$.

relative histogram (lower panel) the "hole" in the region between -1.675 and -1.660 is due to lack of data.

6. Metallicity and correlations

Is stellar activity the only variable playing a role in the definition of the correlation or anti-correlation observed? In Table B.1, it is noticeable that there is a tendency for the eight stars with negative correlation between the $\log R'_{HK}$ and $\log I_{H\alpha}$ indices to have super-solar metallicity. We plotted the histogram of the two populations, the ones with a positive and a negative correlation, against metallicity (Fig. 5). Symbols and colours are the same as the ones presented Fig. 3. In Fig. 5 (upper panel) the median of the negatively correlated stars is not coincident with the medians of both the sample and the positively correlated stars. The histogram shows that, again, there seems to be two

distinct populations of stars: the majority of the stars with positive correlations have negative metallicity while the negatively correlated stars appear to be of super-solar metallicity (mainly if compared to the overall sample). The sample median is -0.10 dex, the positively correlated stars median lie at -0.15 dex, but the negatively correlated stars' median is at a metallicity of 0.20 dex. This is further corroborated by the K-S test, which gives a probability of 0.04% that the two populations are indistinct (with a K-S D value of 0.733). The relative histogram of Fig. 5 (lower panel) confirms this with the negatively correlated stars peaking at the super-solar metallicity while the positively correlated stars peaking at the sub-solar metallicity. Nevertheless, there are some stars with negative correlation that have sub-solar metallicity and stars with positive correlation with super-solar metallicity. We plotted metallicity histograms for two bins where there is superposition of positively and negatively correlated stars in activity in the region $-4.8 \leq \log R'_{HK} \leq -5.0$ (Fig. 6). The tendency for

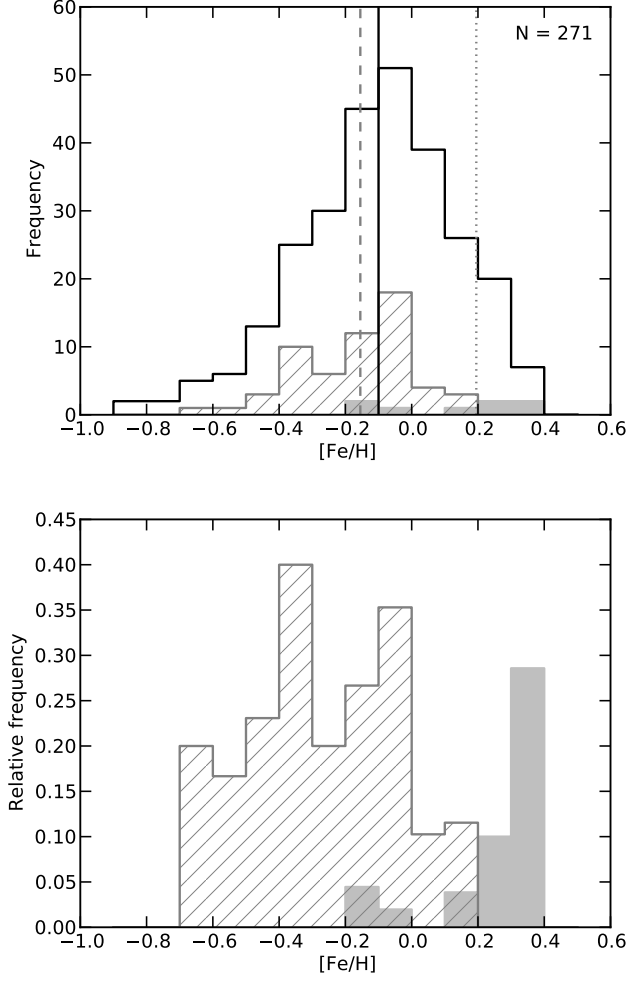


Fig. 5: *Upper panel:* Distribution of metallicity for the full sample (black), stars with positive correlation coefficient higher than 0.5 (hatched grey), and stars with negative correlation coefficient lower than -0.5 (filled grey). Black vertical line is the median of the full sample, dashed vertical line the median of the positively correlated stars, and dotted line the median of the negatively correlated stars. *Lower panel:* Same as the top panel but for relative distributions. The K-S test gives a p-value of 0.01% for the probability that the two populations are drawn from the same distribution.

stars with higher metal content to have negative correlations is maintained in each activity bin. In the lower panel of the figure, for the three stars with metallicity between -0.1 and -0.2 dex, the positively correlated star has $[\text{Fe}/\text{H}] = -0.20$ dex, while the two negatively correlated stars have $[\text{Fe}/\text{H}] = -0.16$ and $[\text{Fe}/\text{H}] = -0.15$ dex. These plots show that for a given activity range, metallicity is still having an impact on the correlation between $\log R'_{HK}$ and $\log I_{H\alpha}$.

Our analysis was based on a small number of anti-correlated stars, and our conclusions can be a consequence of small-number statistics. Also, as was stated before, this sample is not rigorous in terms of long-term variability of the stars or the significance of the correlations used. Further studies with a larger number of metal-rich stars would be crucial to confirm or refute these results.

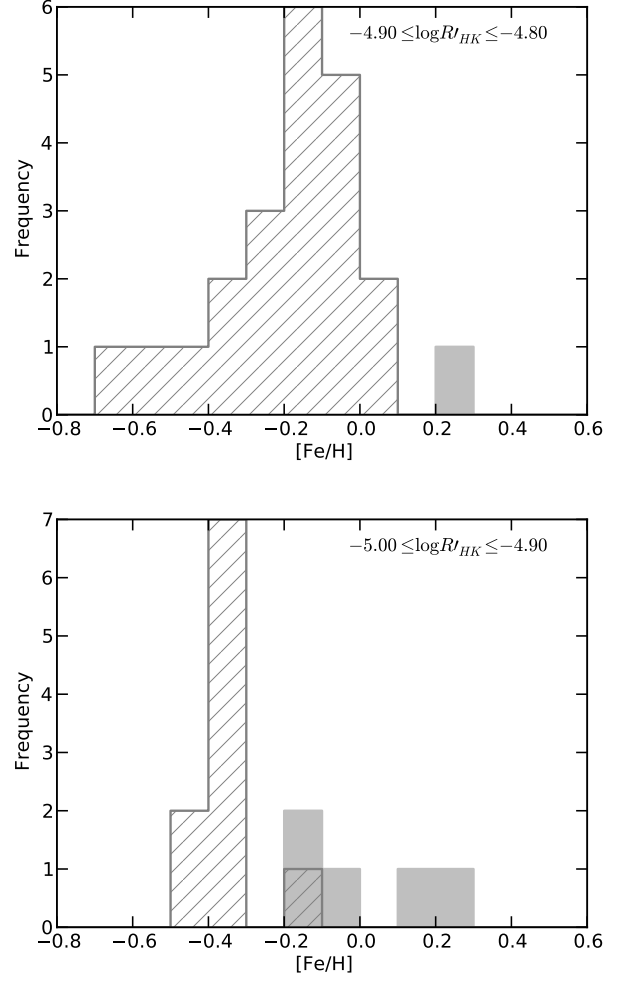


Fig. 6: *Upper panel:* Distribution of metallicity for stars with positive correlation coefficient higher than 0.5 (hatched grey), and stars with negative correlation coefficient lower than -0.5 (filled grey) with activity in the range $-4.9 \leq \log R'_{HK} \leq -4.8$. *Lower panel:* Same as the top panel but for stars with activity in the range $-5.0 \leq \log R'_{HK} \leq -4.9$.

7. Effective temperature and correlations

We also analysed what would be the effect of temperature on the correlations between $\log R'_{HK}$ and $\log I_{H\alpha}$. Figure 7 (upper panel) shows the distributions of the correlations for the full sample (black), the positively correlated stars (hatched grey), and negatively correlated stars (filled grey). Black vertical line is the median of the full sample with a value of 5604 K, dashed vertical line the median of the positively correlated stars with a value of 5243 K, and dotted line the median of the negatively correlated stars with a value of 5386 K. There is an observational bias toward brighter stars and therefore hotter ones. However, the positively correlated stars seem very well distributed across the temperature range, which implies that, relative to the full sample distribution, there are more cooler stars having positive correlations than hotter stars. This can be easily observed in the lower panel of Fig. 7. Stars with negative correlations appear also well distributed in effective temperature, but are only restricted to the range between ~ 5000 and ~ 6100 K. It would be easier then to find positively correlated stars among the cooler dwarfs. This ef-

fect is probably due to the fact that, in our sample, cooler stars have a tendency to be more active than the hotter ones (Fig. 8). All the stars in our sample with $\log R'_{HK} > -4.7$ have effective temperatures lower than 5500 K. And as we saw before in Sect. 5, all stars with activity higher than -4.7 have positive correlations.

Since the Mount Wilson survey, it is known that stellar age and mean activity level are related: younger stars exhibit higher activity levels than their older counterparts (Baliunas et al. 1995). Stars with $0.55 < B - V < 0.9$ which are evolved have lower activity levels than non-evolved stars (do Nascimento et al. 2003). Furthermore, Wright (2004) found that most of the stars classified as "flat" or "Maunder minimum", showing very low activity and no variability, were in fact evolved or subgiant stars. Recently, Schröder et al. (2013) showed that the mean activity level decreases with relative MS-age. This confirms theoretical work by Reiners & Mohanty (2012). In other words, cooler K and M dwarfs did not had enough time to evolve (and decrease their activity level) so much as F-stars which evolve faster. We therefore observe cooler stars at a relative younger stage, and consequently higher activity levels, than their hotter counterparts.

The tendency for more earlier types in our sample will then be a consequence of the bias towards less active stars due to the planetary search nature of this survey.

8. Discussion

8.1. Interpretation of the correlations via the effect of filaments and plages

So, why we sometimes see stars with anti-correlations (and "anti-cycles") when we measure the flux in the H α line? Meunier & Delfosse (2009) studied the contribution of plages and filaments to the S_{MW} and H α indices for the case of the Sun. They noted that the emission in the Ca II lines increases in the presence of plages but is almost unaffected by filaments (their contribution is negligible). On the other hand, filaments contribute to the absorption in the flux of H α while plages contributes to emission. However, the filling factor of filaments saturates at a given activity level while plages filling factor continues to increase as the activity level increases further. This saturation will contribute to an increase of the correlation between the flux in the two line cores for higher activity levels. For the Sun, the filaments are not only found in active regions. They explain that the positive correlation between the two indices is due to the fact that as activity gets stronger (higher emission in the Ca II lines), for the H α index, which is more sensitive to filaments than the Ca II lines, the contribution of plages becomes more important than the contribution coming from filaments, because their contribution saturates at a certain activity level. This will produce the observed strong positive correlation between the two indices for higher activity stars as observed in Fig. 3 and 9. On the other hand, the low-activity stars with anti-correlation between the emission in Ca II and H α , which appear in Fig. 3 and 9, can be explained if these stars have the filaments with a strong contrast (compared to plages) and which not reach the saturation limit.

The occurrence of positively correlated stars at higher activity levels and negatively correlated stars at lower activity levels that we observe in Section 5 can then be explained by the effect of filaments on the flux of the H α line.

If the positively and negatively correlated stars are two different populations in terms of metallicity as discussed in Section 6, and if the ratio of the contrast/filling factor of filaments to plages

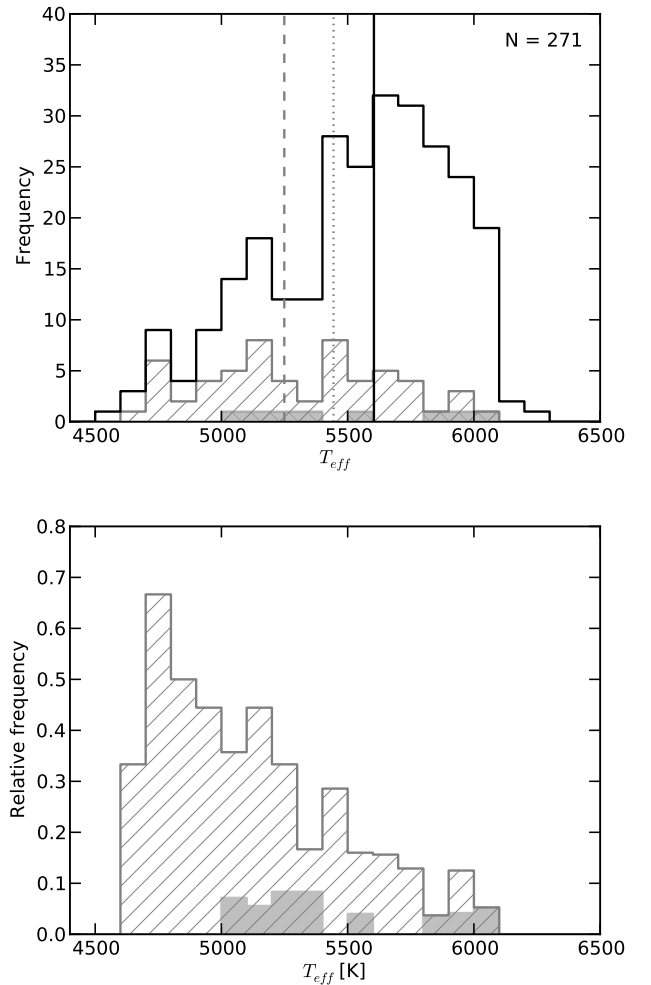


Fig. 7: *Upper panel:* Distribution of effective temperature for the full sample (black), stars with positive correlation coefficient higher than 0.5 (hatched grey), and stars with negative correlation coefficient lower than -0.5 (filled grey). Black vertical line is the median of the full sample, dashed vertical line the median of the positively correlated stars, and dotted line the median of the negatively correlated stars. *Lower panel:* Same as the top panel but for relative distributions.

is responsible for the anti-correlation between the flux in the Ca II H & K and H α lines, then metallicity might have an effect on the presence of filaments (or their contrast and/or filling factor) in the stellar corona. This could be used to predict the correlation between these two indices and to forecast the presence, contrast, and/or filling factor between plages and filaments for a given star.

8.2. Comparison with M dwarfs

In a previous work, Gomes da Silva et al. (2011) studied the long-term activity of 30 M0-M5 dwarfs and found hints of H α "anti-cycles" (inverted in comparison to the $\log R'_{HK}$ cycles) on some stars of their sample. The potential maxima and minima of some stars were anti-correlated. This can be an indication that the physical mechanisms responsible for the anti-correlation, and thus "anti-cycles", between the two indices are present both

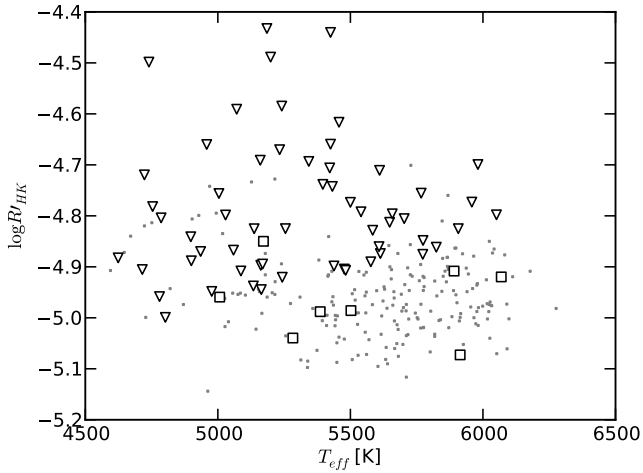


Fig. 8: Activity level measured by $\log R'_{HK}$ against effective temperature. Triangles are stars with $\rho \geq 0.5$ and squares stars with $\rho \leq -0.5$

in solar-type stars and at least in the earlier M dwarfs. The authors also found that after a certain value of S -index activity all M-dwarfs in their sample have positive correlations, and found a case of an anti-correlation with correlation coefficient value lower than -0.5 in the least active stars zone (see their Fig. 3). We should note, however, that their S -index was not corrected for the effects of photospheric flux, and therefore there is a temperature contribution to the mean index values that will vary from star to star. Nevertheless, their distribution of correlations is compatible with ours in the sense that after a certain level of activity all active stars have positive correlations, and there are some cases of low activity stars with anti-correlations (Fig. 9). Since both FGK and early M stars have radiative cores with convective envelopes, their activity phenomena might not be too different (contrary to later M dwarfs which are fully convective). Therefore, if the contribution of filaments to the H α absorption is the sole responsible to the anti-correlation between the flux in the Ca II and H α lines, then it is possible that this phenomenon is occurring in a similar way for the two types of stars.

Further studies of the correlations between the two indices for later M dwarfs would be interesting to understand how the behaviour of the two indices evolve in spectral type and infer about the presence of filaments in fully convective stars.

9. Conclusions

We studied the correlation between the flux in the Ca II H & K and H α lines via two activity indices, R'_{HK} and $I_{H\alpha}$, corrected for photospheric flux. A sample of 271 low activity FGK stars, observed during ~ 9 years, was used to this effect. This study was the larger scale study (in both sample number and time-span) of the correlation between these two chromospheric indices for solar-type stars.

We detected significant activity cycles in 69 stars (26% of our sample) using the $\log R'_{HK}$ index, but only in 9 stars (3.3%) using $\log I_{H\alpha}$. The H α line is not so sensitive at measuring long-term variations as the Ca II lines. We also found a great variety of correlation coefficients, in the range $-0.78 \leq \rho \leq 0.95$, similar to what was found by Cincunegui et al. (2007). Possible explanations for this variety are given by Meunier & Delfosse (2009)

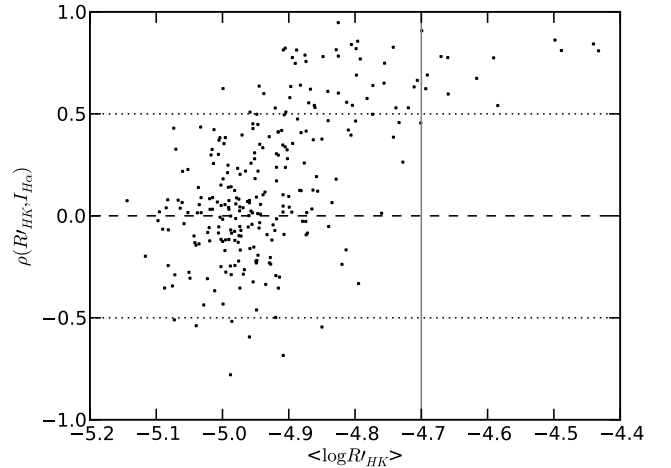


Fig. 9: Correlation coefficient of the relation between $\log R'_{HK}$ and $\log I_{H\alpha}$ against mean $\log R'_{HK}$ level. The vertical line at $\log R'_{HK} = -4.7$ marks the limit after which all stars have positive correlations.

and include the spatial distribution and difference in contrast of filaments relative to plages.

To study the correlation between the $\log R'_{HK}$ and $\log I_{H\alpha}$ indices we first selected only the stars showing "strong" long-term correlations between the two indices by applying a rigorous selection criteria based on variability F-tests, using FAPs on the correlation coefficients and binning the data to 100-day bins. This selection criteria returned a sample of 12 stars where two of them have anti-correlations and the rest positive correlations. We observed that the two stars with anti-correlations have tendency to have lower activity levels and super-solar metallicity when compared to the positively correlated stars.

Since this rigorous selection returned a small number of stars, we relaxed the selection criteria to increase our sample and study the trends found with the rigorous selection. Using this selection criteria we found that:

- 58 stars (21% out of 271) have positive correlations (with $\rho \geq 0.5$) and 8 stars (3% out of 271) show anti-correlations (with $\rho \leq -0.5$). These numbers are compatible with those found by Gomes da Silva et al. (2011) for early-M dwarfs. Some of the stars with strong anti-correlations show "anti-cycles" measured in $\log I_{H\alpha}$: negative activity cycles when compared to those measured by $\log R'_{HK}$.
- The stars with positive correlation between the two indices have a tendency to be more active than those with negative correlations. In fact, all the stars with $\log R'_{HK} \geq -4.7$ have positive correlation between the indices. We interpret this behaviour using Meunier & Delfosse (2009) results that after a certain level of activity, the contribution to absorption in the H α line by filaments saturates, and only plages contribute to emission in both Ca II and H α .
- We also found a tendency for the stars with negative correlations to be more metal rich than the rest of the sample and that this holds for stars of similar activity level.
- The distribution of the correlations in effective temperature was also studied, and we detected that, in relative terms, there are more cooler stars showing positive correlations than hotter stars. This is because, in our sample, cooler stars are in

general more active than hotter ones, and there is a tendency for the more active stars to have positive correlations.

- As a parallel result, we found that our H α index can be used to estimate the effective temperature of a low-activity FGK star.

These results might affect planet detections since activity is one of the main source of errors in radial velocity (and photometric) measurements. It would be interesting to compare the correlation between the flux in the Ca II H & K and H α lines with the measured radial velocity and see if this correlation has any effect on the observed radial velocity signal.

Acknowledgements. This work has been supported by the European Research Council/European Community under the FP7 through a Starting Grant, as well as in the form of a grant reference PTDT/CTE-AST/098528/2008, funded by Fundação para a Ciência e a Tecnologia (FCT), Portugal. J.G.S. would like to thank the financial support given by FCT in the form of a scholarship, namely SFRH/BD/64722/2009. N.C.S. would further like to thank the support from FCT through a Ciência 2007 contract funded by FCT/MCTES (Portugal) and POPH/FSE (EC). I.B. also acknowledges the financial support given by FCT in the form of grant reference SFRH/BPD/81084/2011.

References

- Baliunas, S. L., Donahue, R. A., Soon, W. H., et al. 1995, *ApJ*, 438, 269
Barklem, P. S., Stempels, H. C., Allende Prieto, C., et al. 2002, *A&A*, 385, 951
Boisse, I., Bouchy, F., Hébrard, G., et al. 2011, *A&A*, 528, A4+
Boisse, I., Moutou, C., Vidal-Madjar, A., et al. 2009, *A&A*, 495, 959
Bouchy, F., Queloz, D., Deleuil, M., et al. 2008, *A&A*, 482, L25
Cincunegui, C., Díaz, R. F., & Mauas, P. J. D. 2007, *A&A*, 469, 309
do Nascimento, Jr., J. D., Canto Martins, B. L., Melo, C. H. F., Porto de Mello, G., & De Medeiros, J. R. 2003, *A&A*, 405, 723
Dumusque, X., Lovis, C., Ségransan, D., et al. 2011a, *A&A*, 535, A55
Dumusque, X., Pepe, F., Lovis, C., et al. 2012, *Nature*, 491, 207
Dumusque, X., Santos, N. C., Udry, S., Lovis, C., & Bonfils, X. 2011b, *A&A*, 527, A82
Fuhrmann, K., Axer, M., & Gehren, T. 1993, *A&A*, 271, 451
Giampapa, M. S., Cram, L. E., & Wild, W. J. 1989, *ApJ*, 345, 536
Gomes da Silva, J., Santos, N. C., Bonfils, X., et al. 2011, *A&A*, 534, A30+
Gomes da Silva, J., Santos, N. C., Bonfils, X., et al. 2012, *A&A*, 541, A9
Livingston, W., Wallace, L., White, O. R., & Giampapa, M. S. 2007, *ApJ*, 657, 1137
Lovis, C., Dumusque, X., Santos, N. C., et al. 2011, *ArXiv e-prints*
Meunier, N. & Delfosse, X. 2009, *A&A*, 501, 1103
Montes, D., Fernandez-Figueroa, M. J., de Castro, E., & Cornide, M. 1995, *A&A*, 294, 165
Noyes, R. W., Hartmann, L. W., Baliunas, S. L., Duncan, D. K., & Vaughan, A. H. 1984, *ApJ*, 279, 763
Pasquini, L. & Pallavicini, R. 1991, *A&A*, 251, 199
Queloz, D., Henry, G. W., Sivan, J. P., et al. 2001, *A&A*, 379, 279
Reiners, A. & Mohanty, S. 2012, *ApJ*, 746, 43
Robertson, P., Endl, M., Cochran, W. D., & Dodson-Robinson, S. E. 2013, *ApJ*, 764, 3
Robinson, R. D., Cram, L. E., & Giampapa, M. S. 1990, *ApJS*, 74, 891
Saar, S. H. & Donahue, R. A. 1997, *ApJ*, 485, 319
Santos, N. C., Gomes da Silva, J., Lovis, C., & Melo, C. 2010, *A&A*, 511, A54+
Santos, N. C., Mayor, M., Naef, D., et al. 2000, *A&A*, 361, 265
Santos, N. C., Pont, F., Melo, C., et al. 2006, *A&A*, 450, 825
Schröder, K.-P., Mittag, M., Hempelmann, A., González-Pérez, J. N., & Schmitt, J. H. M. M. 2013, *A&A*, 554, A50
Sousa, S. G., Santos, N. C., Mayor, M., et al. 2008, *A&A*, 487, 373
Sozzetti, A., Torres, G., Charbonneau, D., et al. 2007, *ApJ*, 664, 1190
Sozzetti, A., Torres, G., Charbonneau, D., et al. 2009, *ApJ*, 691, 1145
Strassmeier, K. G., Fekel, F. C., Bopp, B. W., Dempsey, R. C., & Henry, G. W. 1990, *ApJS*, 72, 191
Vaughan, A. H. & Preston, G. W. 1980, *PASP*, 92, 385
Wright, J. T. 2004, *AJ*, 128, 1273
Zechmeister, M., Kürster, M., & Endl, M. 2009, *A&A*, 505, 859

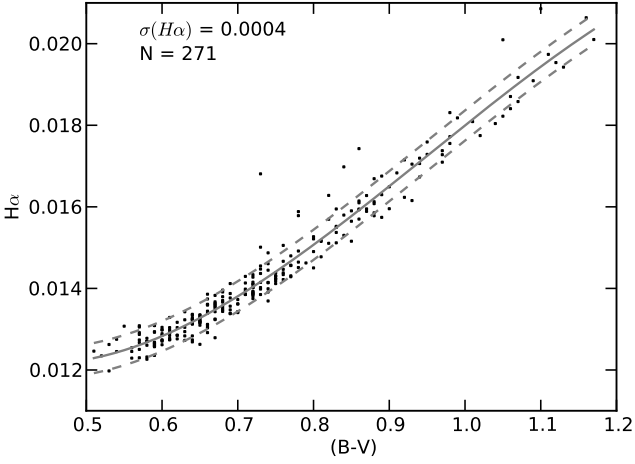


Fig. A.1: Calibration of H α index as a function of $(B-V)$ colour. The solid curve line is the best fit to the data and the dashed lines correspond to the $1-\sigma$ limits.

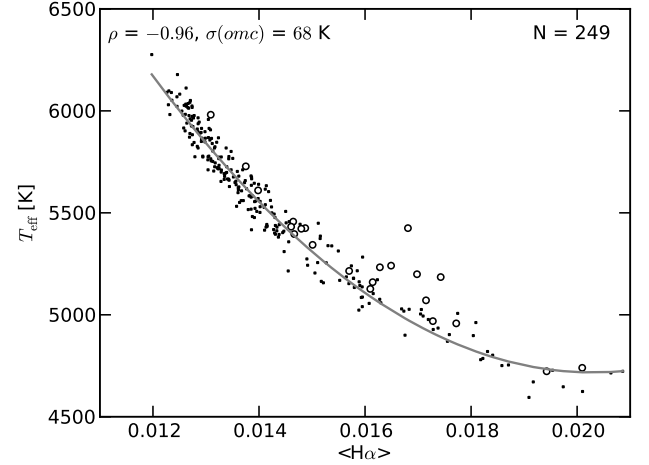


Fig. B.1: Calibration of T_{eff} by using H α activity index for all main sequence stars except the most active ($\log I_{HK} \geq -4.75$, open circles). The grey line is the best quadratic fit to the data.

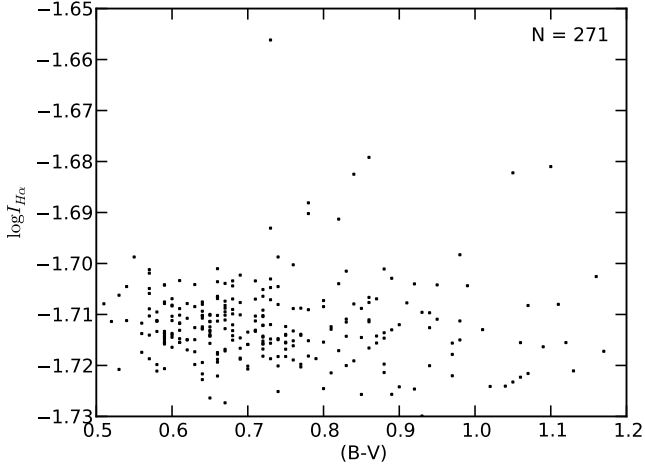


Fig. A.2: Dependence of the $\log I_{H\alpha}$ index on stellar colour.

Appendix A: The $I_{H\alpha}$ hydrogen line based activity index

The H α index is calculated from the fraction of the flux in the H α line centre to the flux in two continuum reference bands, one bluer other redder than the hydrogen line. This is sufficient if we are interested in determining the activity evolution over time for a star. However, stars with different colours have different amounts of flux in the continuum, and this will make the average H α level not comparable between different stars due to a systematic error introduced by the photospheric flux interference in the measurements (e.g. Cincunegui et al. 2007).

To be able to compare the average H α index between different stars the photospheric contribution to the index need to be taken into account. Figure A.1 shows the calibration of H α to the effects of stellar colour. We fitted H α to $(B-V)$ using a cubic polynomial which resulted in a standard deviation of the fit of 0.0004. Our corrected $I_{H\alpha}$ activity index is then

$$I_{H\alpha} = H\alpha + 0.019(B-V)^3 - 0.054(B-V)^2 + 0.037(B-V). \quad (\text{A.1})$$

Figure A.2 shows that the resulting index is not dependent on $(B-V)$ and can therefore be used to compare the activity level of stars of different colour. This calibration is valid for main sequence stars with $(B-V)$ colour between 0.5 and 1.2, and mean H α activity levels between 0.012 and 0.021.

Appendix B: Estimating effective temperature using the flux in H α line

The H α line wings are known to be a proxy of effective temperature (e.g. Fuhrmann et al. 1993; Barklem et al. 2002) and are sometimes used to confirm more accurate results by other methods. For example, Bouchy et al. (2008) used the wings of the H α line to derive a temperature of 5450 ± 120 K for the star CoRoT-Exo-2. Sozzetti et al. (2007) compared the H α wings to those of synthetic spectra to obtain a temperature region of 5750-6000 K for TrES-2 (other authors that used the same technique as a rogue estimate of temperature include Santos et al. 2006; Sozzetti et al. 2009).

We found that our H α activity index is also a good proxy of T_{eff} . Figure B.1 shows a quadratic fit to the correlation between these parameters. Active stars (open circles) were not used due to their contribution to a larger scatter. We obtained an rms of the T_{eff} residuals of $\sigma = 68$ K, and a correlation coefficient of $\rho = -0.96$. The calibrated T_{eff} is of the form

$$T_{\text{eff}} = 10^{-4} (2109 H\alpha^2 - 85.65 H\alpha + 1.341). \quad (\text{B.1})$$

This equation can be used for dwarfs with $\log I_{HK} \leq -4.70$, mean H α activity in the range $0.012 \leq H\alpha \leq 0.021$, and effective temperatures in the range $4600 \leq T_{\text{eff}} \leq 6280$ K.

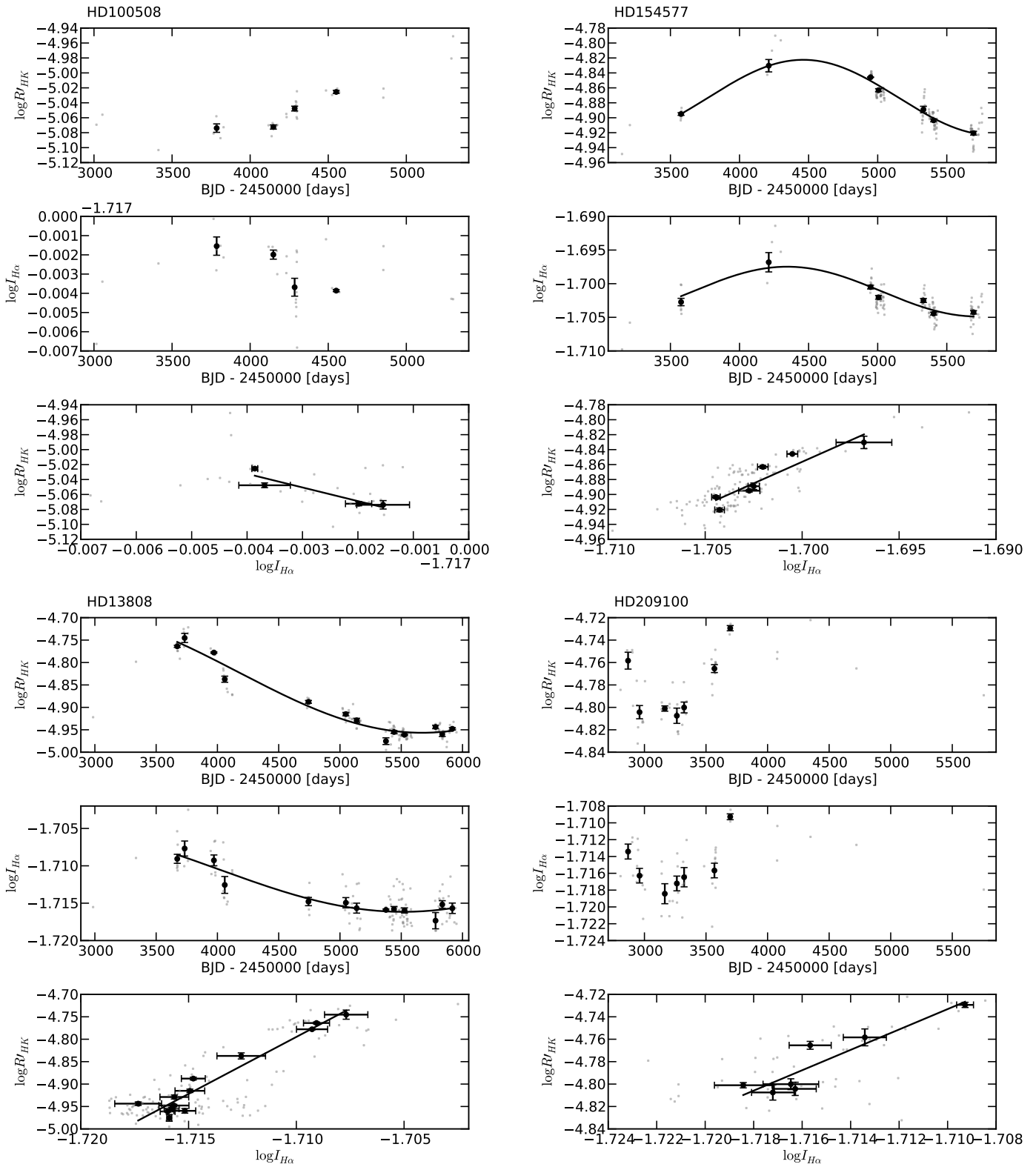


Fig. B.2: Time-series of $\log R'_{HK}$, $\log I_{H\alpha}$, and correlation between the two for the 12 stars with "strong" correlations. Grey dots are nightly averaged data, black points are binned data. Error bars are the standard errors on the mean. Black lines are best fit to the binned data. A sinusoid will appear in the time-series if well fitted, i.e., having $p(F) \leq 0.05$.

Fig. B.2: Continued.

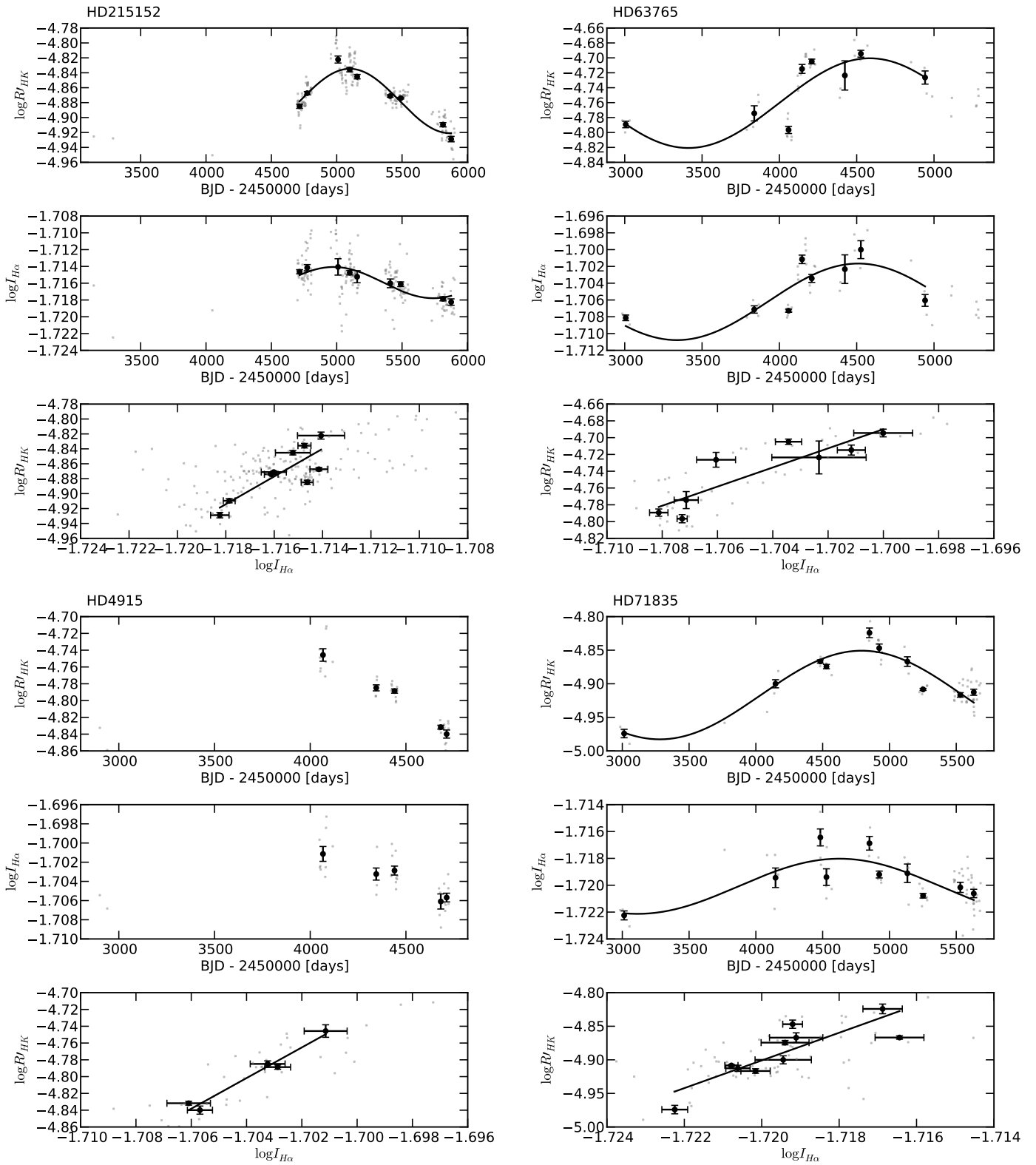


Fig. B.2: Continued.

Fig. B.2: Continued.

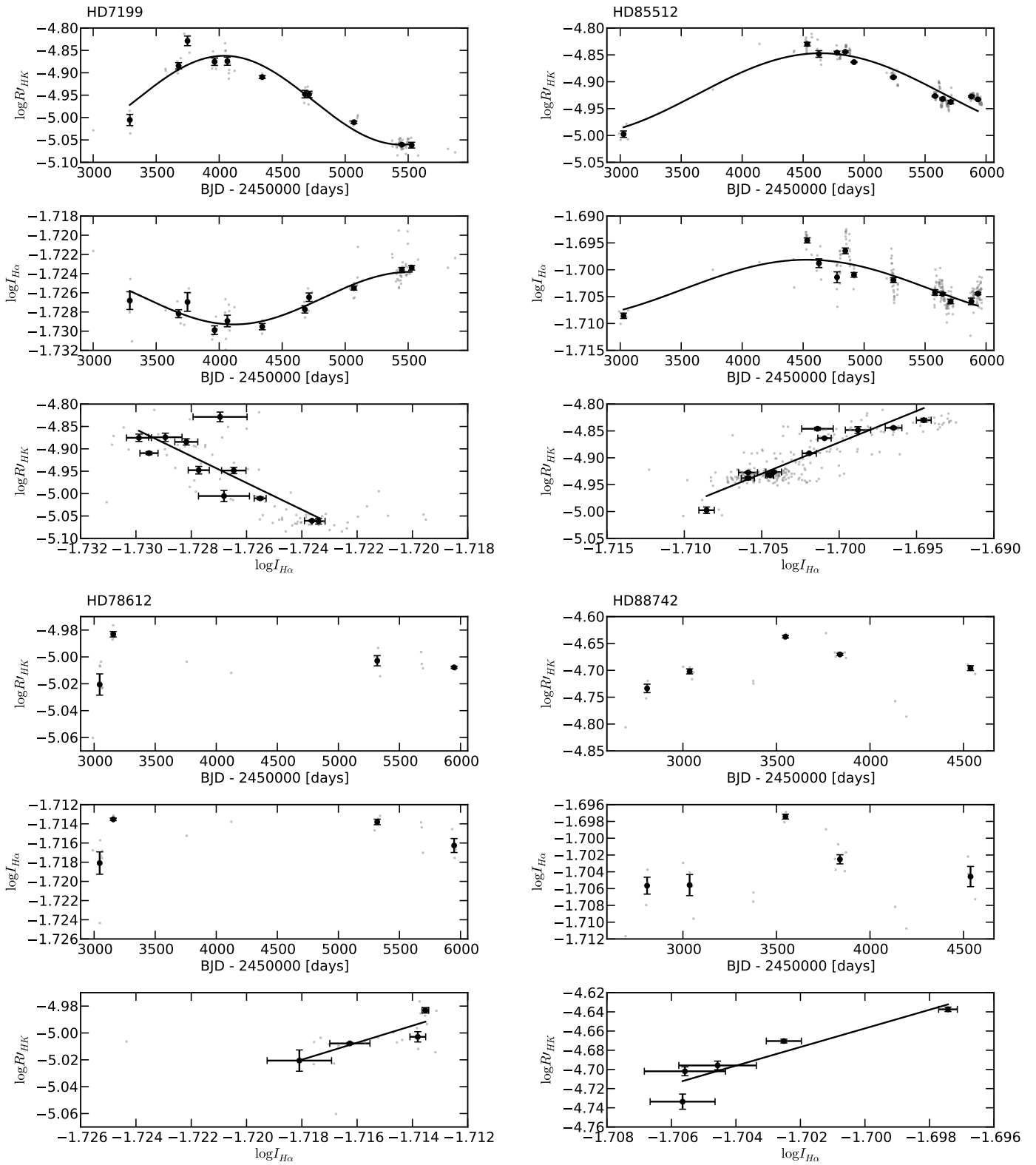


Fig. B.2: Continued.

Fig. B.2: Continued.

Table B.1: Parameters for the 66 stars with $|\rho| \geq 0.5$ from the nightly averaged 271-star sample..

Star	N_{obs}	T_{span} [days]	ρ	[Fe/H]	T_{eff} [K]	$\langle \log R'_{HK} \rangle$	$\sigma(\log R'_{HK})$	$\langle \log I_{H\alpha} \rangle$	$\sigma(\log I_{H\alpha})$
HD105837	21	2651	0.78	-0.51 ± 0.01	5907 ± 17	-4.825	0.019	-1.7012	0.0024
HD106275	17	2648	0.62	-0.09 ± 0.03	5059 ± 45	-4.867	0.065	-1.7130	0.0037
HD109200	118	2866	0.60	-0.31 ± 0.02	5134 ± 38	-4.938	0.033	-1.7079	0.0023
HD110619	17	2677	0.76	-0.41 ± 0.01	5613 ± 15	-4.874	0.019	-1.7065	0.0019
HD114747	32	1472	-0.55	0.21 ± 0.04	5172 ± 57	-4.850	0.073	-1.7246	0.0027
HD119638	31	3276	-0.50	-0.15 ± 0.01	6069 ± 16	-4.920	0.015	-1.7112	0.0017
HD119782	14	2194	0.69	-0.07 ± 0.02	5160 ± 34	-4.691	0.020	-1.7067	0.0028
HD124364	13	2635	0.81	-0.27 ± 0.01	5584 ± 14	-4.828	0.037	-1.7039	0.0025
HD125072	24	2173	-0.59	0.18 ± 0.07	5007 ± 103	-4.959	0.052	-1.7241	0.0025
HD125455	17	2164	0.63	-0.18 ± 0.02	5162 ± 41	-4.897	0.043	-1.7156	0.0032
HD13060	18	2522	0.60	0.02 ± 0.03	5255 ± 45	-4.825	0.061	-1.7073	0.0023
HD130992	18	1830	0.61	-0.13 ± 0.06	4898 ± 75	-4.841	0.022	-1.7241	0.0037
HD13789	10	397	0.86	-0.06 ± 0.06	4740 ± 71	-4.498	0.026	-1.6822	0.0049
HD13808	128	2964	0.81	-0.20 ± 0.03	5087 ± 41	-4.908	0.074	-1.7142	0.0033
HD140901	24	1545	0.63	0.09 ± 0.01	5610 ± 21	-4.711	0.032	-1.7103	0.0019
HD14374	17	1804	0.60	-0.04 ± 0.02	5425 ± 24	-4.659	0.031	-1.6987	0.0034
HD144585	14	2538	-0.51	0.33 ± 0.02	5914 ± 22	-5.073	0.019	-1.7188	0.0020
HD145666	20	1410	0.64	-0.04 ± 0.01	5958 ± 12	-4.773	0.014	-1.7069	0.0015
HD148303	25	2162	0.78	-0.03 ± 0.06	4958 ± 91	-4.660	0.041	-1.7113	0.0051
HD154577	123	2606	0.81	-0.70 ± 0.02	4900 ± 37	-4.888	0.030	-1.7029	0.0025
HD157830	50	2624	0.77	-0.25 ± 0.01	5540 ± 16	-4.792	0.033	-1.7023	0.0031
HD162236	14	965	0.62	-0.12 ± 0.02	5343 ± 25	-4.693	0.030	-1.6931	0.0032
HD16297	10	2052	0.66	-0.01 ± 0.02	5422 ± 22	-4.706	0.031	-1.7088	0.0033
HD172513	40	1081	0.50	-0.05 ± 0.01	5500 ± 18	-4.774	0.020	-1.7154	0.0019
HD18386	14	405	0.67	0.14 ± 0.02	5457 ± 29	-4.616	0.039	-1.7152	0.0036
HD18719	12	340	0.54	-0.08 ± 0.02	5241 ± 32	-4.585	0.015	-1.7120	0.0044
HD188559	25	1145	0.54	-0.11 ± 0.04	4786 ± 100	-4.804	0.055	-1.7233	0.0044
HD19034	18	2962	0.51	-0.48 ± 0.01	5477 ± 15	-4.904	0.018	-1.7044	0.0018
HD192961	11	2690	0.64	-0.35 ± 0.04	4624 ± 73	-4.882	0.033	-1.7172	0.0040
HD197210	12	2218	0.75	-0.03 ± 0.01	5577 ± 20	-4.890	0.022	-1.7133	0.0018
HD197823	18	1056	0.53	0.12 ± 0.02	5396 ± 32	-4.738	0.051	-1.7088	0.0023
HD206172	11	2550	0.53	-0.24 ± 0.01	5608 ± 14	-4.860	0.029	-1.7074	0.0025
HD20619	26	2138	0.84	-0.22 ± 0.01	5703 ± 13	-4.806	0.032	-1.7069	0.0033
HD208272	28	527	0.81	-0.08 ± 0.03	5199 ± 40	-4.489	0.020	-1.6825	0.0049
HD209100	49	2949	0.58	-0.20 ± 0.04	4754 ± 89	-4.782	0.028	-1.7155	0.0033
HD209742	11	2911	0.95	-0.16 ± 0.03	5137 ± 49	-4.825	0.049	-1.7111	0.0031
HD215152	194	2761	0.55	-0.10 ± 0.04	4935 ± 76	-4.870	0.033	-1.7156	0.0025
HD21749	47	2224	0.53	-0.02 ± 0.08	4723 ± 143	-4.720	0.042	-1.7211	0.0046
HD219249	26	2942	0.50	-0.40 ± 0.01	5482 ± 13	-4.907	0.017	-1.7077	0.0010
HD220339	10	2122	0.82	-0.35 ± 0.03	5029 ± 52	-4.798	0.049	-1.7011	0.0037
HD222237	18	1513	0.51	-0.38 ± 0.04	4780 ± 64	-4.958	0.037	-1.7044	0.0027
HD222595	26	1334	0.56	0.01 ± 0.01	5648 ± 16	-4.813	0.055	-1.7135	0.0022
HD224393	11	2560	0.78	-0.38 ± 0.01	5774 ± 17	-4.848	0.028	-1.7034	0.0021
HD224789	33	2833	0.81	-0.03 ± 0.02	5185 ± 38	-4.433	0.020	-1.6792	0.0063
HD23356	11	2227	0.65	-0.17 ± 0.03	5004 ± 60	-4.756	0.015	-1.7096	0.0038
HD27063	39	1575	0.75	0.05 ± 0.01	5767 ± 14	-4.756	0.018	-1.7111	0.0014
HD34688	11	2713	0.78	-0.20 ± 0.02	5169 ± 39	-4.895	0.062	-1.7109	0.0038
HD40307	193	2990	0.50	-0.31 ± 0.03	4977 ± 59	-4.948	0.056	-1.7097	0.0034
HD44573	25	2353	0.77	-0.07 ± 0.03	5071 ± 56	-4.591	0.029	-1.7040	0.0038
HD4915	39	1822	0.86	-0.21 ± 0.01	5658 ± 13	-4.796	0.037	-1.7036	0.0025
HD63765	46	2302	0.83	-0.16 ± 0.01	5432 ± 19	-4.742	0.039	-1.7046	0.0031
HD65277	18	2974	0.62	-0.31 ± 0.04	4802 ± 88	-4.999	0.034	-1.7223	0.0022
HD67458	25	3158	-0.68	-0.16 ± 0.01	5891 ± 12	-4.908	0.018	-1.7104	0.0026
HD70889	16	1579	0.69	0.11 ± 0.01	6051 ± 15	-4.798	0.033	-1.7145	0.0026
HD71835	70	2697	0.58	-0.04 ± 0.02	5438 ± 22	-4.898	0.035	-1.7198	0.0018
HD7199	84	2872	-0.78	0.28 ± 0.03	5386 ± 45	-4.988	0.081	-1.7257	0.0027
HD72673	66	3025	0.53	-0.41 ± 0.01	5243 ± 22	-4.920	0.027	-1.7091	0.0020
HD80883	13	526	0.78	-0.25 ± 0.03	5233 ± 35	-4.670	0.042	-1.6913	0.0055
HD8389A	13	2998	-0.54	0.34 ± 0.05	5283 ± 64	-5.040	0.030	-1.7242	0.0027
HD85119	19	480	0.84	-0.20 ± 0.02	5425 ± 25	-4.440	0.015	-1.6562	0.0043
HD85512	242	2973	0.82	-0.32 ± 0.03	4715 ± 102	-4.905	0.041	-1.7026	0.0039
HD8859	16	2914	-0.52	-0.09 ± 0.01	5502 ± 18	-4.986	0.011	-1.7122	0.0021
HD88742	24	1868	0.91	-0.02 ± 0.01	5981 ± 13	-4.699	0.045	-1.7042	0.0040
HD90812	17	2306	0.64	-0.36 ± 0.02	5164 ± 35	-4.945	0.039	-1.7124	0.0025
HD92719	21	2941	0.54	-0.10 ± 0.01	5824 ± 16	-4.861	0.024	-1.7079	0.0014
HD95521	19	2968	0.79	-0.15 ± 0.01	5773 ± 18	-4.875	0.041	-1.7103	0.0019

Table B.2: Parameters for the 205 stars with $|\rho| \leq 0.5$ from the nightly averaged 271-star sample.

Star	N_{obs}	T_{span} [days]	ρ	[Fe/H]	T_{eff} [K]	$\langle \log R'_{HK} \rangle$	$\sigma(\log R'_{HK})$	$\langle \log I_{H\alpha} \rangle$	$\sigma(\log I_{H\alpha})$
HD10002	12	838	0.08	0.17 ± 0.03	5313 ± 44	-5.083	0.013	-1.7115	0.0019
HD100508	32	2283	-0.31	0.39 ± 0.05	5449 ± 61	-5.049	0.030	-1.7200	0.0015
HD10180	220	2974	-0.08	0.08 ± 0.01	5911 ± 19	-5.006	0.013	-1.7173	0.0018
HD102365	33	2965	-0.03	-0.29 ± 0.02	5629 ± 29	-4.944	0.010	-1.7102	0.0015
HD102438	39	2243	-0.22	-0.29 ± 0.01	5560 ± 13	-4.950	0.008	-1.7090	0.0018
HD104006	24	2232	0.00	-0.78 ± 0.02	5023 ± 37	-4.960	0.011	-1.6881	0.0016
HD104067	86	2270	0.39	-0.06 ± 0.05	4969 ± 72	-4.742	0.025	-1.7178	0.0030
HD104263	27	2244	-0.13	0.02 ± 0.02	5477 ± 23	-5.042	0.021	-1.7141	0.0023
HD104982	40	2270	-0.32	-0.19 ± 0.01	5692 ± 14	-4.954	0.010	-1.7101	0.0019
HD106116	106	2697	-0.31	0.14 ± 0.01	5680 ± 15	-5.023	0.011	-1.7159	0.0021
HD10700	230	3125	0.08	-0.52 ± 0.01	5310 ± 17	-4.959	0.006	-1.7047	0.0012
HD108309	21	2676	0.08	0.12 ± 0.01	5775 ± 14	-5.019	0.017	-1.7273	0.0012
HD111031	26	2244	0.08	0.27 ± 0.02	5801 ± 22	-5.067	0.009	-1.7166	0.0012
HD11226	28	1766	0.05	0.04 ± 0.01	6098 ± 14	-5.002	0.005	-1.7187	0.0022
HD114853	36	3031	-0.34	-0.23 ± 0.01	5705 ± 14	-4.935	0.017	-1.7124	0.0032
HD11505	17	2944	-0.02	-0.22 ± 0.01	5752 ± 10	-5.000	0.005	-1.7128	0.0012
HD115585	17	2640	-0.20	0.35 ± 0.02	5711 ± 29	-5.116	0.013	-1.7251	0.0014
HD115617	142	2910	-0.12	-0.02 ± 0.01	5558 ± 19	-4.990	0.010	-1.7113	0.0015
HD115674	38	2251	0.10	-0.17 ± 0.01	5649 ± 20	-4.900	0.015	-1.7101	0.0015
HD117105	18	2657	0.45	-0.29 ± 0.01	5889 ± 14	-4.947	0.006	-1.7113	0.0018
HD117207	16	2680	0.22	0.22 ± 0.02	5667 ± 21	-5.060	0.004	-1.7157	0.0013
HD122862	17	2294	0.09	-0.12 ± 0.01	5982 ± 13	-5.015	0.007	-1.7198	0.0009
HD123265	16	2641	-0.02	0.19 ± 0.03	5338 ± 44	-5.097	0.011	-1.7143	0.0022
HD12345	15	2472	0.21	-0.21 ± 0.02	5395 ± 29	-4.992	0.010	-1.7139	0.0011
HD12387	15	2838	0.06	-0.24 ± 0.01	5700 ± 18	-4.980	0.009	-1.7114	0.0013
HD124292	28	3100	-0.12	-0.13 ± 0.02	5443 ± 22	-4.995	0.011	-1.7120	0.0029
HD125881	24	3002	0.02	0.06 ± 0.01	6036 ± 17	-4.873	0.024	-1.7137	0.0015
HD126525	48	2805	-0.24	-0.10 ± 0.01	5638 ± 13	-4.981	0.007	-1.7120	0.0018
HD128674	19	2262	0.41	-0.38 ± 0.01	5551 ± 15	-4.916	0.007	-1.7082	0.0014
HD129642	45	1085	0.07	-0.06 ± 0.04	5026 ± 76	-4.962	0.019	-1.7126	0.0018
HD130930	14	1781	0.30	0.01 ± 0.03	5027 ± 61	-5.017	0.015	-1.7077	0.0010
HD1320	13	1957	-0.09	-0.27 ± 0.01	5679 ± 14	-4.874	0.016	-1.7100	0.0009
HD132648	27	2623	0.47	-0.37 ± 0.01	5418 ± 16	-4.841	0.033	-1.7064	0.0035
HD134060	105	2897	-0.13	0.14 ± 0.01	5966 ± 14	-5.000	0.009	-1.7150	0.0018
HD134606	121	2448	-0.07	0.27 ± 0.02	5633 ± 28	-5.082	0.008	-1.7150	0.0016
HD134664	27	1066	0.41	0.10 ± 0.01	5865 ± 19	-4.881	0.027	-1.7178	0.0016
HD136352	148	2809	-0.23	-0.34 ± 0.01	5664 ± 14	-4.949	0.005	-1.7080	0.0017
HD136713	41	2202	-0.33	0.07 ± 0.05	4994 ± 74	-4.795	0.038	-1.7220	0.0022
HD136894	37	2044	-0.28	-0.10 ± 0.02	5412 ± 22	-4.995	0.005	-1.7051	0.0016
HD13724	26	2134	0.01	0.23 ± 0.02	5868 ± 27	-4.760	0.026	-1.7172	0.0025
HD137388	30	2148	0.36	0.18 ± 0.03	5240 ± 53	-4.894	0.049	-1.7257	0.0024
HD138549	22	2621	0.18	0.00 ± 0.01	5582 ± 19	-4.828	0.044	-1.7152	0.0021
HD1388	64	3025	0.09	-0.01 ± 0.01	5954 ± 10	-4.979	0.007	-1.7140	0.0016
HD142709	13	2523	0.18	-0.35 ± 0.03	4728 ± 65	-4.999	0.051	-1.7155	0.0022
HD143114	19	1789	-0.19	-0.41 ± 0.01	5775 ± 18	-4.946	0.005	-1.7088	0.0012
HD144628	51	2105	0.28	-0.41 ± 0.02	5085 ± 34	-4.952	0.022	-1.7114	0.0020
HD145598	32	2107	0.30	-0.78 ± 0.02	5417 ± 21	-4.916	0.011	-1.7010	0.0018
HD1461	193	3027	-0.06	0.19 ± 0.01	5765 ± 18	-5.020	0.013	-1.7128	0.0014
HD146233	51	2602	-0.20	0.04 ± 0.01	5818 ± 13	-4.928	0.025	-1.7142	0.0014
HD14747	14	2860	-0.06	-0.39 ± 0.01	5516 ± 16	-4.945	0.018	-1.7070	0.0020
HD147512	29	1734	0.08	-0.08 ± 0.01	5530 ± 15	-4.990	0.006	-1.7121	0.0014
HD150433	58	2223	-0.05	-0.36 ± 0.01	5665 ± 12	-4.961	0.005	-1.7041	0.0016
HD151504	14	1897	0.01	0.06 ± 0.02	5457 ± 31	-5.038	0.004	-1.7139	0.0019
HD15337	29	1975	-0.35	0.06 ± 0.03	5179 ± 44	-4.916	0.038	-1.7214	0.0017
HD154088	124	2014	0.04	0.28 ± 0.03	5374 ± 43	-5.064	0.015	-1.7129	0.0020
HD154363	19	2529	-0.24	-0.62 ± 0.04	4723 ± 89	-4.820	0.050	-1.6810	0.0043
HD157172	82	2266	0.06	0.11 ± 0.02	5451 ± 27	-4.996	0.036	-1.7182	0.0020
HD157338	24	1460	0.04	-0.08 ± 0.01	6027 ± 13	-4.969	0.010	-1.7154	0.0017
HD157347	20	2892	0.26	0.02 ± 0.01	5676 ± 16	-5.014	0.006	-1.7132	0.0017
HD1581	130	2624	0.12	-0.18 ± 0.01	5977 ± 12	-4.936	0.007	-1.7095	0.0009
HD161098	75	2015	0.42	-0.27 ± 0.01	5560 ± 15	-4.911	0.021	-1.7099	0.0017
HD161612	31	2154	0.09	0.16 ± 0.02	5616 ± 22	-5.032	0.006	-1.7182	0.0015
HD162396	39	1884	-0.17	-0.35 ± 0.01	6090 ± 19	-4.973	0.010	-1.7114	0.0014
HD165920	18	2326	0.04	0.29 ± 0.04	5339 ± 55	-5.085	0.014	-1.7191	0.0021
HD166724	19	2567	0.46	-0.09 ± 0.03	5127 ± 52	-4.734	0.026	-1.7077	0.0035
HD16714	24	2089	0.22	-0.20 ± 0.01	5518 ± 18	-4.965	0.008	-1.7133	0.0018
HD168871	25	2951	-0.01	-0.09 ± 0.01	5983 ± 13	-4.980	0.009	-1.7149	0.0018
HD170493	12	2101	-0.17	0.14 ± 0.11	4751 ± 08	-4.814	0.061	-1.7216	0.0029
HD171665	12	1730	0.34	-0.05 ± 0.01	5655 ± 12	-4.906	0.017	-1.7146	0.0018
HD174545	13	2574	-0.23	0.22 ± 0.04	5216 ± 57	-4.929	0.041	-1.7198	0.0017
HD176986	79	2625	0.06	0.00 ± 0.03	5018 ± 59	-4.835	0.024	-1.7201	0.0026
HD177409	16	1979	0.37	-0.04 ± 0.01	5898 ± 10	-4.863	0.028	-1.7083	0.0012
HD177565	26	1684	0.33	0.08 ± 0.01	5627 ± 19	-4.939	0.041	-1.7159	0.0026
HD177758	10	2834	0.39	-0.58 ± 0.02	5862 ± 23	-4.929	0.003	-1.7049	0.0015

Table B.2: Continued.

Star	N_{obs}	T_{span} [days]	ρ	[Fe/H]	T_{eff} [K]	$\langle \log R'_{HK} \rangle$	$\sigma(\log R'_{HK})$	$\langle \log I_{H\alpha} \rangle$	$\sigma(\log I_{H\alpha})$
HD17970	19	2962	0.07	-0.45 ± 0.04	5040 ± 48	-5.008	0.012	-1.7015	0.0023
HD180409	11	2834	-0.12	-0.17 ± 0.01	6013 ± 18	-4.925	0.004	-1.7103	0.0015
HD181433	123	3011	0.07	0.33 ± 0.13	4962 ± 34	-5.144	0.014	-1.7130	0.0023
HD183658	16	2171	0.14	0.03 ± 0.01	5803 ± 17	-4.987	0.008	-1.7128	0.0022
HD183783	11	2676	-0.09	-0.20 ± 0.07	4595 ± 73	-4.907	0.049	-1.7163	0.0020
HD185615	19	2297	-0.10	0.08 ± 0.02	5570 ± 20	-5.043	0.014	-1.7156	0.0016
HD188748	20	2133	-0.26	-0.12 ± 0.01	5623 ± 17	-4.967	0.013	-1.7088	0.0018
HD189567	174	2941	0.41	-0.24 ± 0.01	5726 ± 15	-4.916	0.016	-1.7142	0.0014
HD189625	16	1743	0.42	0.18 ± 0.02	5846 ± 22	-4.810	0.041	-1.7133	0.0025
HD190248	136	2942	0.02	0.33 ± 0.03	5604 ± 38	-5.095	0.010	-1.7168	0.0010
HD190954	11	2204	-0.29	-0.41 ± 0.02	5430 ± 24	-4.969	0.012	-1.7070	0.0022
HD192031	11	519	0.45	-0.84 ± 0.01	5215 ± 16	-4.954	0.006	-1.7030	0.0019
HD192310	206	3082	0.14	-0.04 ± 0.03	5166 ± 49	-4.991	0.040	-1.7136	0.0017
HD193193	30	1134	-0.09	-0.05 ± 0.01	5979 ± 13	-4.933	0.016	-1.7158	0.0018
HD19467	21	2941	0.15	-0.14 ± 0.01	5720 ± 10	-5.002	0.015	-1.7131	0.0019
HD196761	10	2822	0.17	-0.31 ± 0.01	5415 ± 16	-4.918	0.025	-1.7102	0.0026
HD199190	23	762	0.23	0.15 ± 0.01	5926 ± 17	-5.052	0.014	-1.7198	0.0014
HD199288	16	2602	0.02	-0.63 ± 0.01	5765 ± 19	-4.895	0.005	-1.7042	0.0013
HD199960	28	854	-0.37	0.28 ± 0.02	5973 ± 26	-5.012	0.019	-1.7217	0.0013
HD20003	104	2280	-0.25	0.04 ± 0.02	5494 ± 27	-4.988	0.040	-1.7203	0.0014
HD203432	33	1405	0.19	0.29 ± 0.02	5645 ± 25	-4.858	0.057	-1.7201	0.0022
HD20407	20	3062	0.04	-0.44 ± 0.01	5866 ± 14	-4.899	0.007	-1.7078	0.0010
HD204313	70	2026	0.03	0.18 ± 0.02	5776 ± 22	-5.019	0.017	-1.7202	0.0015
HD204385	13	2889	-0.13	0.07 ± 0.01	6033 ± 16	-4.976	0.009	-1.7164	0.0014
HD204941	38	2546	0.31	-0.19 ± 0.03	5056 ± 52	-4.952	0.030	-1.7146	0.0020
HD205536	22	2218	0.33	-0.05 ± 0.02	5442 ± 23	-5.016	0.006	-1.7152	0.0020
HD207129	79	1875	0.32	0.00 ± 0.01	5937 ± 13	-4.903	0.030	-1.7112	0.0016
HD207700	13	2111	0.30	0.04 ± 0.01	5666 ± 18	-5.006	0.010	-1.7207	0.0015
HD20781	124	2966	-0.14	-0.11 ± 0.02	5256 ± 29	-5.035	0.011	-1.7171	0.0022
HD20782	55	2983	0.30	-0.06 ± 0.01	5774 ± 14	-4.919	0.015	-1.7149	0.0019
HD20794	279	3033	-0.12	-0.40 ± 0.01	5401 ± 17	-4.981	0.006	-1.7034	0.0018
HD207970	12	2955	-0.44	0.07 ± 0.02	5556 ± 25	-5.028	0.010	-1.7148	0.0016
HD20807	39	2308	0.12	-0.23 ± 0.01	5866 ± 11	-4.881	0.013	-1.7082	0.0017
HD208704	12	2638	0.02	-0.09 ± 0.01	5826 ± 11	-4.957	0.011	-1.7194	0.0019
HD210752	14	2534	-0.03	-0.57 ± 0.01	5923 ± 23	-4.874	0.004	-1.7045	0.0018
HD210918	31	1857	-0.25	-0.09 ± 0.01	5755 ± 12	-5.002	0.015	-1.7157	0.0013
HD211415	13	2997	0.24	-0.21 ± 0.01	5850 ± 14	-4.919	0.023	-1.7117	0.0012
HD21209A	12	3022	-0.05	-0.41 ± 0.04	4671 ± 65	-4.840	0.022	-1.7082	0.0024
HD212708	30	1058	-0.34	0.27 ± 0.02	5681 ± 27	-5.076	0.014	-1.7187	0.0020
HD213628	12	2608	0.26	0.01 ± 0.01	5555 ± 20	-4.957	0.010	-1.7145	0.0025
HD213941	26	2217	0.35	-0.46 ± 0.01	5532 ± 18	-4.909	0.013	-1.7095	0.0023
HD214385	11	2911	-0.04	-0.34 ± 0.01	5654 ± 15	-4.924	0.016	-1.7094	0.0016
HD21693	141	2951	0.02	0.00 ± 0.02	5430 ± 26	-4.909	0.055	-1.7161	0.0021
HD21938	18	3019	0.10	-0.47 ± 0.01	5778 ± 18	-4.939	0.007	-1.7076	0.0021
HD220256	22	1217	-0.08	-0.10 ± 0.03	5144 ± 48	-5.022	0.016	-1.7088	0.0013
HD220507	48	2220	0.02	0.01 ± 0.01	5698 ± 17	-5.052	0.010	-1.7186	0.0019
HD221356	23	2941	-0.29	-0.20 ± 0.03	6112 ± 37	-4.919	0.004	-1.7062	0.0010
HD222669	46	1403	0.13	0.05 ± 0.01	5894 ± 17	-4.863	0.022	-1.7118	0.0022
HD224619	15	2992	-0.10	-0.20 ± 0.01	5436 ± 16	-4.975	0.013	-1.7148	0.0012
HD22879	50	2686	0.05	-0.83 ± 0.02	5857 ± 27	-4.908	0.007	-1.6987	0.0015
HD23456	20	2200	0.10	-0.32 ± 0.01	6178 ± 18	-4.909	0.010	-1.7079	0.0019
HD26965A	24	2998	0.35	-0.31 ± 0.03	5153 ± 38	-4.944	0.034	-1.7040	0.0027
HD283	11	2592	-0.46	-0.54 ± 0.02	5157 ± 28	-4.949	0.011	-1.7085	0.0018
HD28471	17	2683	0.04	-0.05 ± 0.01	5745 ± 14	-4.991	0.021	-1.7140	0.0018
HD28701	17	1263	-0.08	-0.32 ± 0.01	5710 ± 12	-4.986	0.012	-1.7114	0.0011
HD28821	18	2904	0.08	-0.12 ± 0.01	5660 ± 13	-4.975	0.013	-1.7151	0.0025
HD30278	21	1513	-0.05	-0.17 ± 0.02	5394 ± 29	-5.006	0.013	-1.7124	0.0019
HD30306	21	2904	0.43	0.17 ± 0.02	5529 ± 26	-5.074	0.013	-1.7156	0.0020
HD31527	182	3011	0.01	-0.17 ± 0.01	5898 ± 13	-4.955	0.006	-1.7131	0.0018
HD31822	43	2352	0.03	-0.19 ± 0.01	6042 ± 16	-4.865	0.007	-1.7113	0.0018
HD32724	21	2954	0.02	-0.17 ± 0.01	5818 ± 13	-5.032	0.013	-1.7150	0.0011
HD33725	17	3011	-0.10	-0.17 ± 0.02	5274 ± 30	-4.972	0.035	-1.7154	0.0015
HD34449	13	2626	0.12	-0.09 ± 0.01	5848 ± 17	-4.883	0.013	-1.7102	0.0017
HD35854	17	2958	0.47	-0.13 ± 0.03	4928 ± 56	-4.799	0.037	-1.7110	0.0038
HD36003	57	1494	-0.08	-0.20 ± 0.06	4647 ± 88	-4.872	0.040	-1.7080	0.0032
HD36108	23	3275	0.25	-0.21 ± 0.01	5916 ± 12	-4.992	0.006	-1.7156	0.0030
HD36379	45	2341	-0.22	-0.17 ± 0.01	6030 ± 14	-4.976	0.006	-1.7174	0.0018
HD37986	19	2975	-0.24	0.26 ± 0.03	5507 ± 38	-5.082	0.013	-1.7245	0.0021
HD3823	33	2265	-0.00	-0.28 ± 0.01	6022 ± 14	-4.988	0.007	-1.7137	0.0010
HD38277	10	3019	-0.12	-0.07 ± 0.01	5871 ± 10	-5.019	0.007	-1.7228	0.0013
HD38858	66	3009	-0.01	-0.22 ± 0.01	5733 ± 12	-4.918	0.013	-1.7102	0.0015
HD38973	22	2353	-0.07	0.05 ± 0.01	6016 ± 17	-4.972	0.013	-1.7138	0.0010
HD39194	156	3008	0.18	-0.61 ± 0.02	5205 ± 23	-4.951	0.014	-1.7003	0.0015
HD40397	21	3060	0.42	-0.13 ± 0.01	5527 ± 20	-5.013	0.009	-1.7104	0.0014

Table B.2: Continued.

Star	N_{obs}	T_{span} [days]	ρ	[Fe/H]	T_{eff} [K]	$\langle \log R'_{HK} \rangle$	$\sigma(\log R'_{HK})$	$\langle \log I_{H\alpha} \rangle$	$\sigma(\log I_{H\alpha})$
HD44120	18	3019	0.33	0.12 ± 0.01	6052 ± 15	-5.070	0.017	-1.7206	0.0010
HD44420	17	2898	0.14	0.29 ± 0.02	5818 ± 22	-5.036	0.024	-1.7188	0.0012
HD44447	23	2989	0.23	-0.22 ± 0.01	5999 ± 14	-4.977	0.015	-1.7117	0.0015
HD44594	21	2903	-0.01	0.15 ± 0.01	5840 ± 14	-5.004	0.020	-1.7175	0.0024
HD45184	102	3013	0.24	0.04 ± 0.01	5869 ± 14	-4.905	0.026	-1.7126	0.0013
HD45289	16	3023	0.44	-0.02 ± 0.01	5717 ± 18	-5.033	0.008	-1.7169	0.0024
HD45364	62	2917	-0.16	-0.17 ± 0.01	5434 ± 20	-4.959	0.022	-1.7092	0.0021
HD47186	104	2879	-0.28	0.23 ± 0.02	5675 ± 21	-5.051	0.009	-1.7131	0.0014
HD50590	12	2193	-0.05	-0.22 ± 0.04	4870 ± 67	-4.974	0.032	-1.7150	0.0021
HD51608	126	2966	0.12	-0.07 ± 0.01	5358 ± 22	-4.982	0.020	-1.7141	0.0023
HD55693	27	3278	-0.43	0.29 ± 0.02	5914 ± 26	-4.999	0.020	-1.7221	0.0028
HD59468	141	2754	-0.17	0.03 ± 0.01	5618 ± 20	-4.996	0.012	-1.7101	0.0010
HD59711A	16	2911	0.22	-0.12 ± 0.01	5722 ± 13	-4.946	0.010	-1.7107	0.0013
HD65562	15	2945	0.43	-0.10 ± 0.03	5076 ± 47	-4.954	0.035	-1.7069	0.0018
HD65907A	61	2608	-0.30	-0.31 ± 0.01	5945 ± 16	-4.914	0.010	-1.7059	0.0013
HD66221	17	2350	-0.04	0.17 ± 0.02	5635 ± 25	-5.058	0.020	-1.7158	0.0028
HD6735	17	2960	0.26	-0.06 ± 0.01	6082 ± 15	-4.877	0.014	-1.7141	0.0012
HD68607	29	1209	0.26	0.07 ± 0.03	5215 ± 45	-4.728	0.036	-1.7166	0.0024
HD68978A	60	2339	-0.03	0.04 ± 0.02	5965 ± 22	-4.879	0.015	-1.7169	0.0018
HD69655	21	2905	0.06	-0.18 ± 0.01	5961 ± 12	-4.943	0.009	-1.7112	0.0014
HD71334	21	2973	-0.29	-0.09 ± 0.01	5694 ± 13	-4.987	0.010	-1.7076	0.0016
HD7134	16	1767	0.09	-0.29 ± 0.01	5940 ± 14	-4.949	0.005	-1.7142	0.0015
HD71479	21	2974	-0.14	0.24 ± 0.01	6026 ± 18	-5.040	0.015	-1.7264	0.0020
HD72579	23	2974	-0.35	0.20 ± 0.02	5449 ± 30	-5.087	0.009	-1.7187	0.0018
HD72769	21	2703	-0.07	0.30 ± 0.02	5640 ± 27	-5.090	0.015	-1.7183	0.0022
HD73121	19	2708	0.07	0.09 ± 0.01	6091 ± 16	-5.061	0.013	-1.7211	0.0021
HD73524	64	2975	-0.12	0.16 ± 0.01	6017 ± 13	-5.002	0.017	-1.7137	0.0014
HD74014	17	2963	-0.29	0.22 ± 0.02	5561 ± 27	-5.072	0.010	-1.7189	0.0008
HD7449	84	2926	0.38	-0.11 ± 0.01	6024 ± 13	-4.850	0.015	-1.7089	0.0015
HD78429	57	1960	-0.24	0.09 ± 0.01	5760 ± 19	-4.927	0.029	-1.7194	0.0023
HD78558	20	2969	0.04	-0.44 ± 0.01	5711 ± 18	-4.974	0.009	-1.7108	0.0023
HD78612	22	2968	0.37	-0.24 ± 0.01	5834 ± 14	-5.005	0.017	-1.7155	0.0025
HD78747	42	2553	-0.07	-0.67 ± 0.01	5778 ± 18	-4.921	0.008	-1.7019	0.0008
HD81639	18	2706	0.03	-0.17 ± 0.02	5522 ± 20	-4.990	0.013	-1.7143	0.0019
HD82342	27	3008	0.01	-0.54 ± 0.03	4820 ± 61	-4.943	0.032	-1.6983	0.0030
HD82516	53	2319	-0.04	0.01 ± 0.04	5104 ± 60	-4.955	0.044	-1.7299	0.0026
HD83529	22	2706	0.40	-0.22 ± 0.01	5902 ± 12	-4.970	0.009	-1.7133	0.0020
HD8406	14	3002	0.12	-0.10 ± 0.01	5726 ± 12	-4.856	0.009	-1.7113	0.0010
HD85390	63	2965	0.06	-0.07 ± 0.03	5186 ± 54	-4.959	0.026	-1.7145	0.0022
HD86140	10	2699	0.40	-0.25 ± 0.04	4903 ± 59	-4.806	0.020	-1.7042	0.0017
HD8638	33	1826	-0.15	-0.38 ± 0.02	5507 ± 26	-4.953	0.006	-1.7034	0.0016
HD88084	18	2692	0.20	-0.10 ± 0.01	5766 ± 11	-4.973	0.009	-1.7124	0.0016
HD8828	45	2223	0.38	-0.16 ± 0.02	5403 ± 25	-4.996	0.010	-1.7080	0.0020
HD89454	48	1467	0.46	0.12 ± 0.01	5728 ± 17	-4.701	0.029	-1.7182	0.0024
HD90156	83	2937	0.01	-0.24 ± 0.01	5599 ± 12	-4.947	0.006	-1.7066	0.0016
HD90711	17	2305	0.38	0.24 ± 0.03	5444 ± 39	-5.004	0.034	-1.7215	0.0021
HD93385	136	2908	-0.07	0.02 ± 0.01	5977 ± 18	-4.988	0.007	-1.7133	0.0019
HD94151	21	2724	0.02	0.04 ± 0.01	5583 ± 19	-4.974	0.031	-1.7168	0.0015
HD95456	77	2338	-0.08	0.16 ± 0.02	6276 ± 22	-4.982	0.019	-1.7208	0.0014
HD96423	22	2722	0.05	0.10 ± 0.01	5711 ± 18	-5.035	0.013	-1.7142	0.0021
HD96700	168	3270	-0.22	-0.18 ± 0.01	5845 ± 13	-4.948	0.011	-1.7148	0.0017
HD97037	18	2668	0.35	-0.07 ± 0.01	5883 ± 14	-4.998	0.009	-1.7155	0.0013
HD97343	21	2695	0.03	-0.06 ± 0.01	5410 ± 20	-5.015	0.009	-1.7132	0.0019
HD9782	27	2216	-0.35	0.09 ± 0.01	6023 ± 19	-4.974	0.007	-1.7146	0.0011
HD9796	15	2573	0.42	-0.25 ± 0.02	5179 ± 28	-4.874	0.025	-1.6902	0.0017
HD97998	17	2351	0.28	-0.42 ± 0.01	5716 ± 21	-4.902	0.007	-1.7085	0.0016
HD98281	54	2226	0.47	-0.26 ± 0.02	5381 ± 23	-4.887	0.027	-1.7071	0.0023